

Massively Parallel Selection of NanoCluster Beacons

Yu-An Kuo¹, Cheulhee Jung³, Yu-An Chen¹, Hung-Che Kuo^{2,4}, Oliver S. Zhao¹, Trung D. Nguyen¹, James R. Rybarski^{2,4}, Soonwoo Hong¹, Yuan-I Chen¹, Dennis C. Wylie⁶, John A. Hawkins⁵, Jada N. Walker⁷, Samuel W. Shields⁷, Jennifer S. Brodbelt⁷, Jeffrey T. Petty⁸, Ilya J. Finkelstein^{2, 4}, and Hsin-Chih Yeh^{1, 9,*}

¹Department of Biomedical Engineering, University of Texas at Austin, Austin, USA

²Department of Molecular Biosciences, University of Texas at Austin, Austin, USA

³Department of Biotechnology, College of Life Sciences and Biotechnology, Korea University, Seoul, Korea

⁴Center for Systems and Synthetic Biology, University of Texas at Austin, Austin, USA

⁵European Molecular Biology Laboratory (EMBL), Heidelberg, Germany

⁶Computational Biology and Bioinformatics, Center for Biomedical Research Support, University of Texas at Austin, Austin, USA

⁷Department of Chemistry, University of Texas at Austin, Austin, USA

⁸Department of Chemistry, Furman University, Greenville, USA

⁹Texas Materials Institute, University of Texas at Austin, Austin, USA

Contents

Figure S1: Schematic of NCB working principle.....	2
Figure S2: Schematic of volumetric integrated intensity.....	2
Figure S3: <i>MiSeq</i> chip images before and after flat-field correction.....	3
Figure S4: Alignment of PhiX fiducial markers.....	4
Figure S5: Identification of activator sequences from the FASTQ data.....	5
Figure S6: <i>MiSeq</i> chip images before and after restriction enzyme digestion.....	6
Figure S7: NCB images before and after restriction enzyme digestion.....	7
Figure S8: Illumination comparison of canonical NCB with different activator length.....	8
Figure S9: Intensity comparison of NCBs on the chip under different hybridization temperature.....	8
Figure S10: Batch to batch variations in <i>MiSeq</i> chip selection for library_1.....	9
Figure S11: Batch to batch variations in <i>MiSeq</i> chip selection for library_2 and library_3.....	10
Figure S12: Titration curve of G15 intensity on the chip.....	11
Figure S13: NCB intensity decay on the chip.....	11
Figure S14: Influence of activator mutations on NCB brightness	12
Figure S15: Nine-segment interrogation on the library_1 design.....	14
Figure S16: Fluorescence correlation spectroscopy (FCS) results on the red NCBs.....	15
Figure S17: Fluorescence correlation spectroscopy (FCS) results on the yellow NCBs.....	16
Figure S18: Small-scale test-tube investigation of G15 twin NCBs in the yellow channel.....	17
Figure S19: Absorption spectra of selected NCBs and POT.....	18
Figure S20: Native PAGE gel photo under UV excitation.....	18
Figure S21: ESI-MS analysis of selective NCBs.....	19
Figure S22: 2D spectra of bright red activator candidates.....	20
Figure S23: 2D spectra of dark activator candidates	21
Figure S24: 2D spectra of bright yellow activator candidates.....	22

Figure S25: 2D spectra of activators with various numbers of guanine bases.....	23
Figure S26: 2D spectra of rationally designed red NCBs.....	24
Figure S27: 2D spectra of rationally designed yellow NCBs.....	25
Figure S28: 2D spectra of randomly designed NCBs	26
Figure S29: 2D spectra of G5 NCBs.....	27
Figure S30: 2D spectra of red POT candidates.....	28
Figure S31: 2D spectra of yellow POT candidates.....	29
Figure S32: 2D spectra of red NCBs near rank 3600.....	30
Figure S33: 2D spectra of yellow NCBs near rank 3600.....	30
Figure S34: Workflow for establishing machine learning models to classify screened NCBs or NCB candidates.....	31
Figure S35: Workflow to rationally design bright NCBs.....	32
Figure S36: CHAMP workflow.....	33
Figure S37: Motif distribution for the top 1,000 library sequences for red and yellow channels.....	34
Table S1: Sequences of probes and library designs used in this report.....	35
Table S2: Test-tube investigation of selected bright red and dark activator candidates.....	38
Table S3: Test-tube investigation of selected bright yellow activator candidates.....	40
Table S4: Test-tube investigation of 10-guanine activators.....	41
Table S5: Test-tube investigation of 12-guanine activators	42
Table S6: Test-tube investigation of rationally designed bright red NCBs	43
Table S7: Test-tube investigation of rationally designed bright yellow NCBs.....	44
Table S8: Test-tube investigation of randomly designed NCBs and G5.....	45
Table S9: Test-tube investigation of red and yellow NCBs ranked near 3600.....	46
Table S10: Test-tube investigation of red POT candidates.....	47
Table S11: Test-tube investigation of yellow POT candidates.....	48
Table S12: Machine learning model prediction results.....	49
Table S13: Selected bright and dark features for yellow channel	50
Table S14: Selected bright and dark features for red channel.....	51
References.....	52

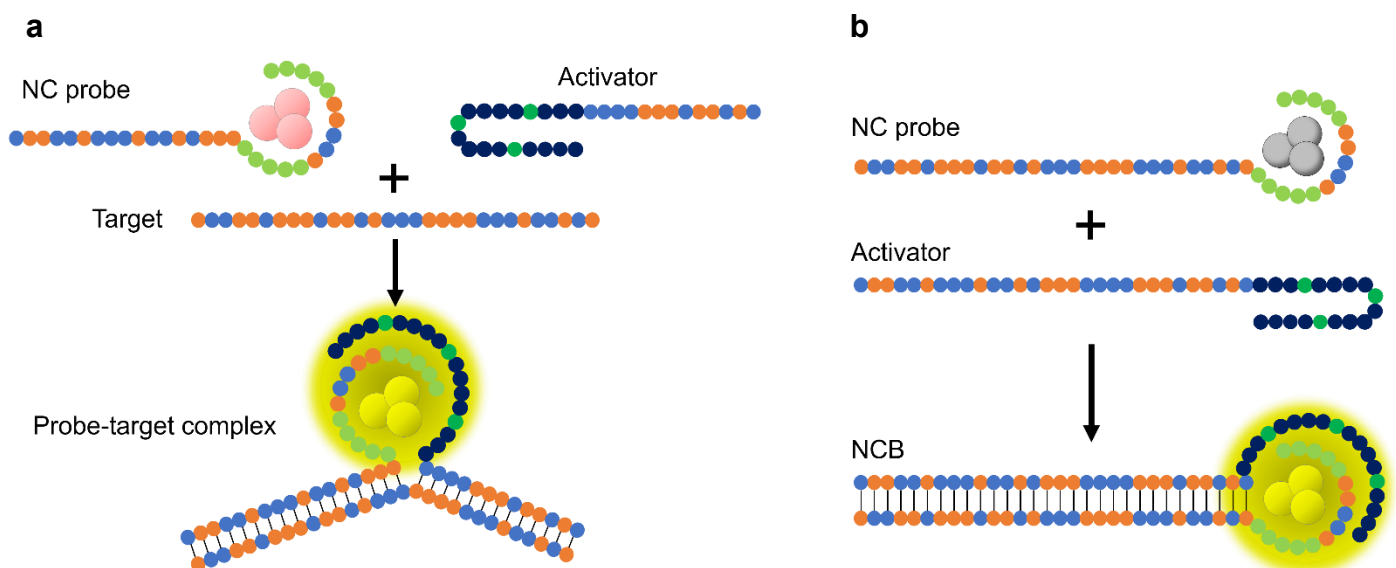


Figure S1 | Schematic of NanoCluster Beacon (NCB) working principle. **a** An NCB consists of an NC probe and an activator probe¹⁻⁵. Upon binding to a target, the dark silver nanocluster (AgNC) interacts with the activator and lights up. NCBs remain dark when there is no target in the solution. **b** In the study, we eliminated the target and only focused on the interactions between the NC probe and the activator.

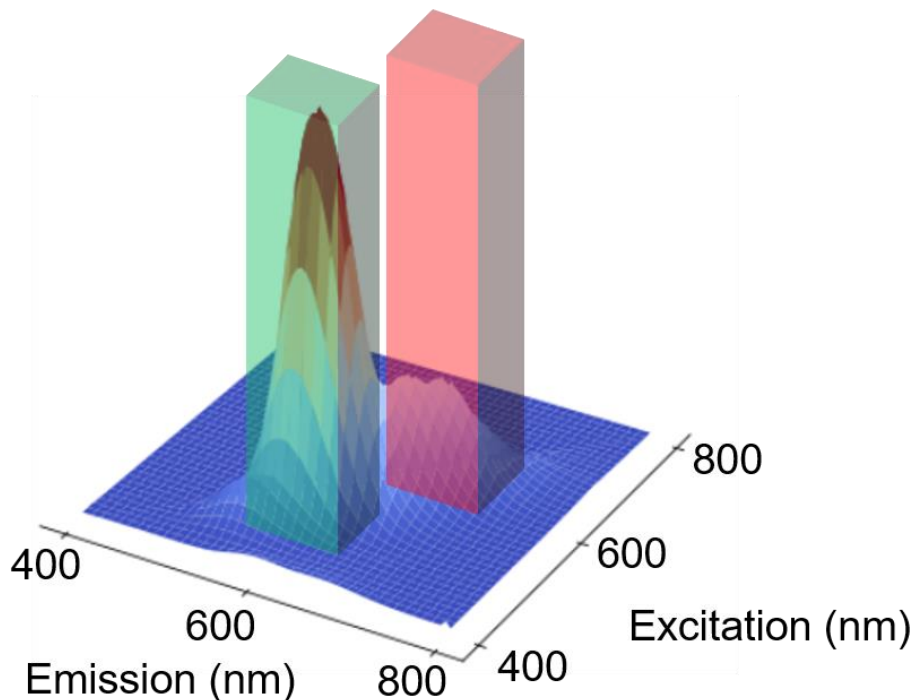
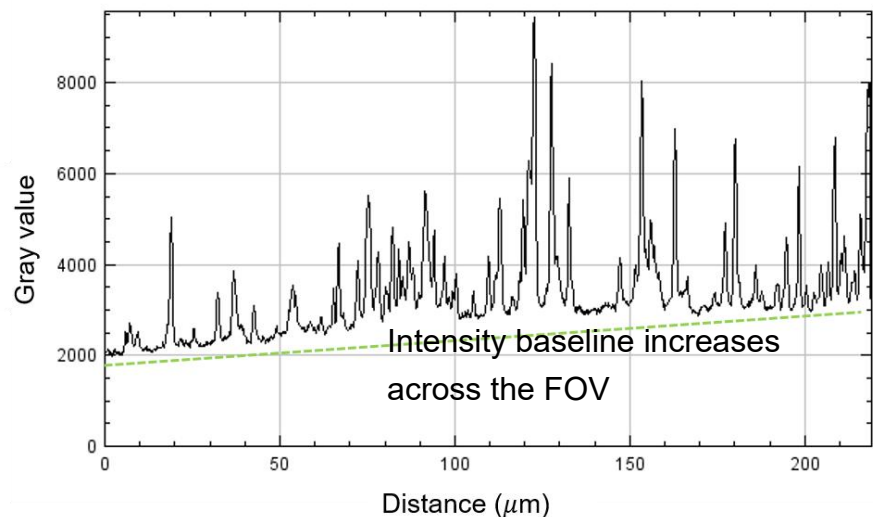
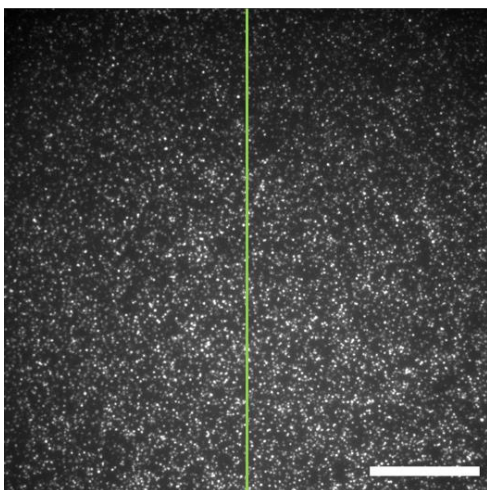
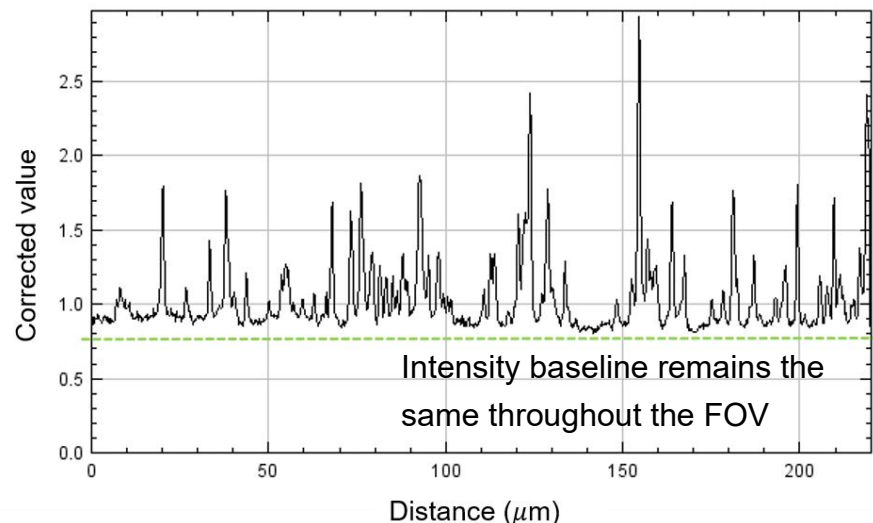
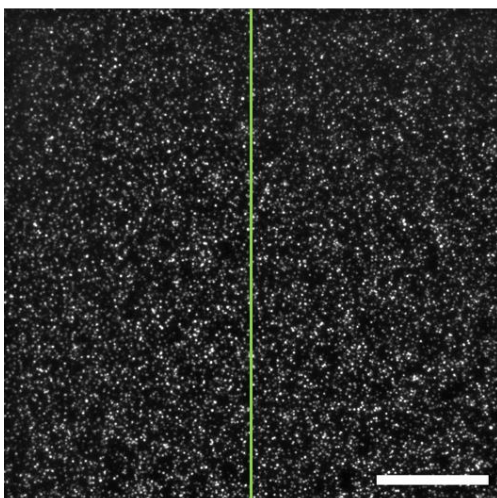


Figure S2 | Schematic of volumetric integrated intensity. From each 2D fluorescence spectrum, we can calculate the volumetric integrated intensities in the yellow channel (Ex/Em: 535/50, 605/70 nm) and the red channel (Ex/Em: 620/60, 700/75 nm), respectively. The volumetric integrated intensity refers to the volumetric integral under the 2D spectrum surface.

a Before pseudo-flat field correction



b After pseudo-flat field correction



c Schematic of a *MiSeq* chip

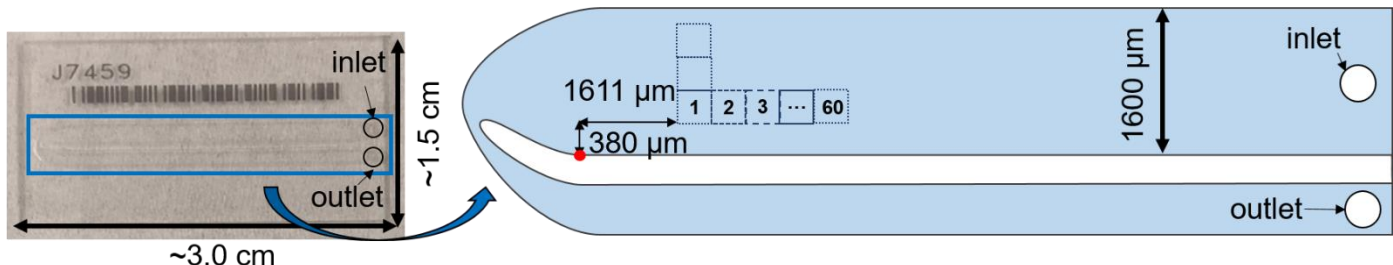


Figure S3 | MiSeq chip images before and after flat-field correction. **a** A representative field-of-view (FOV, $1,024 \times 1,024$ pixel) shows uneven illumination that leads to inconsistent intensity baseline across the FOV. **b** The same FOV is corrected using a pseudo-flat field correction method. The intensity baseline is uniform throughout the FOV after correction. Distance: from top to bottom. Scale bar: $50 \mu\text{m}$. **c** A MiSeq chip is 1.5 cm long and 3.0 cm wide (left). To bypass most of these unregistered regions, we shifted the imaging starting position by $380 \mu\text{m}$ vertically and $1,611 \mu\text{m}$ horizontally with respect to the reference point (red dot) at the bottom left corner (right).

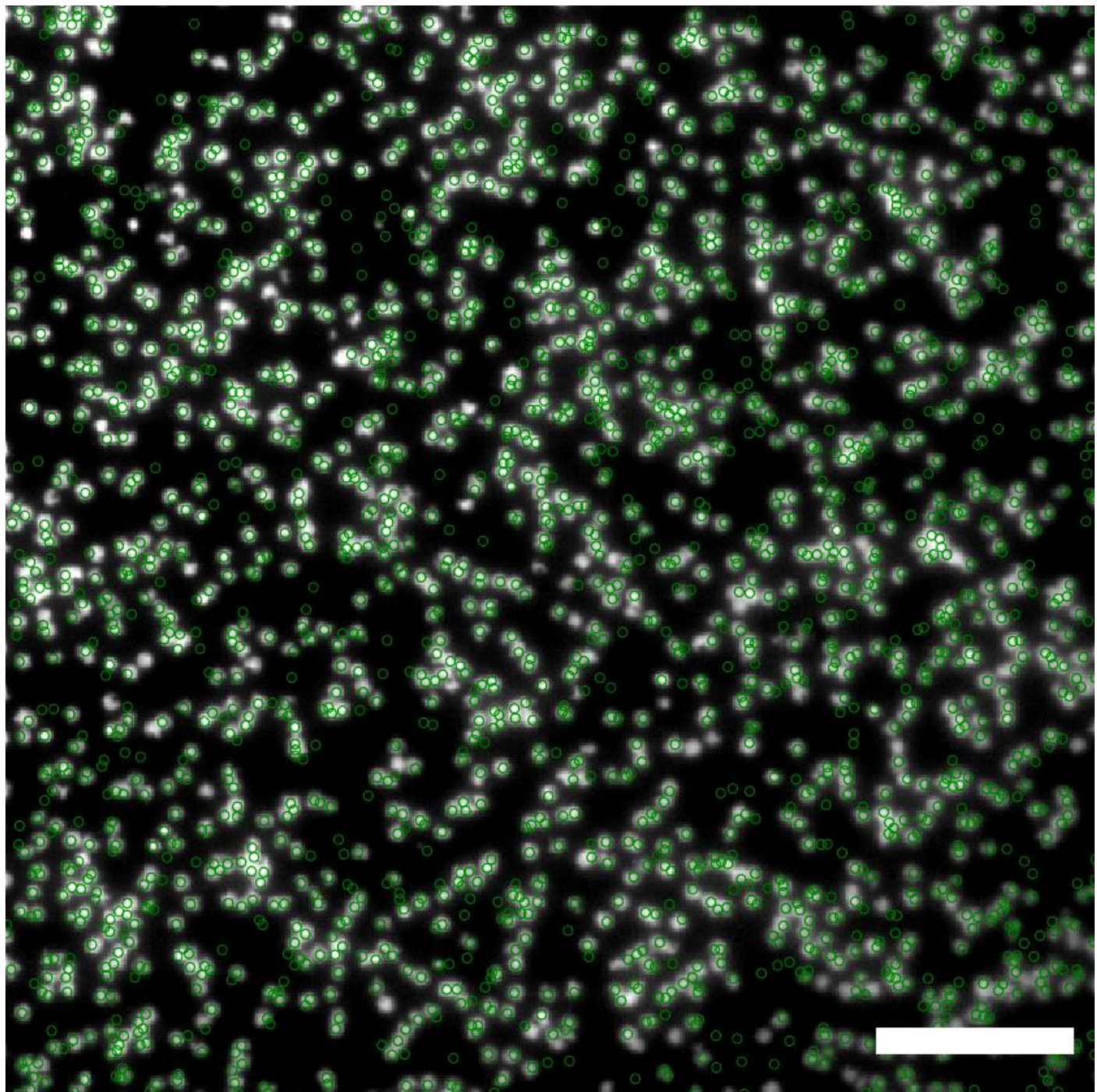


Figure S4 | Alignment of PhiX fiducial markers. A representative FOV (512×512 pixel; 110×110 μm^2) of aligned PhiX fiducial markers acquired under the green channel (EX/EM: 480/40, 535/50 nm). The PhiX fiducial markers are labeled with Atto488 and the registered PhiX positions from the FASTQ data file are circled in green. Scale bar: 20 μm .

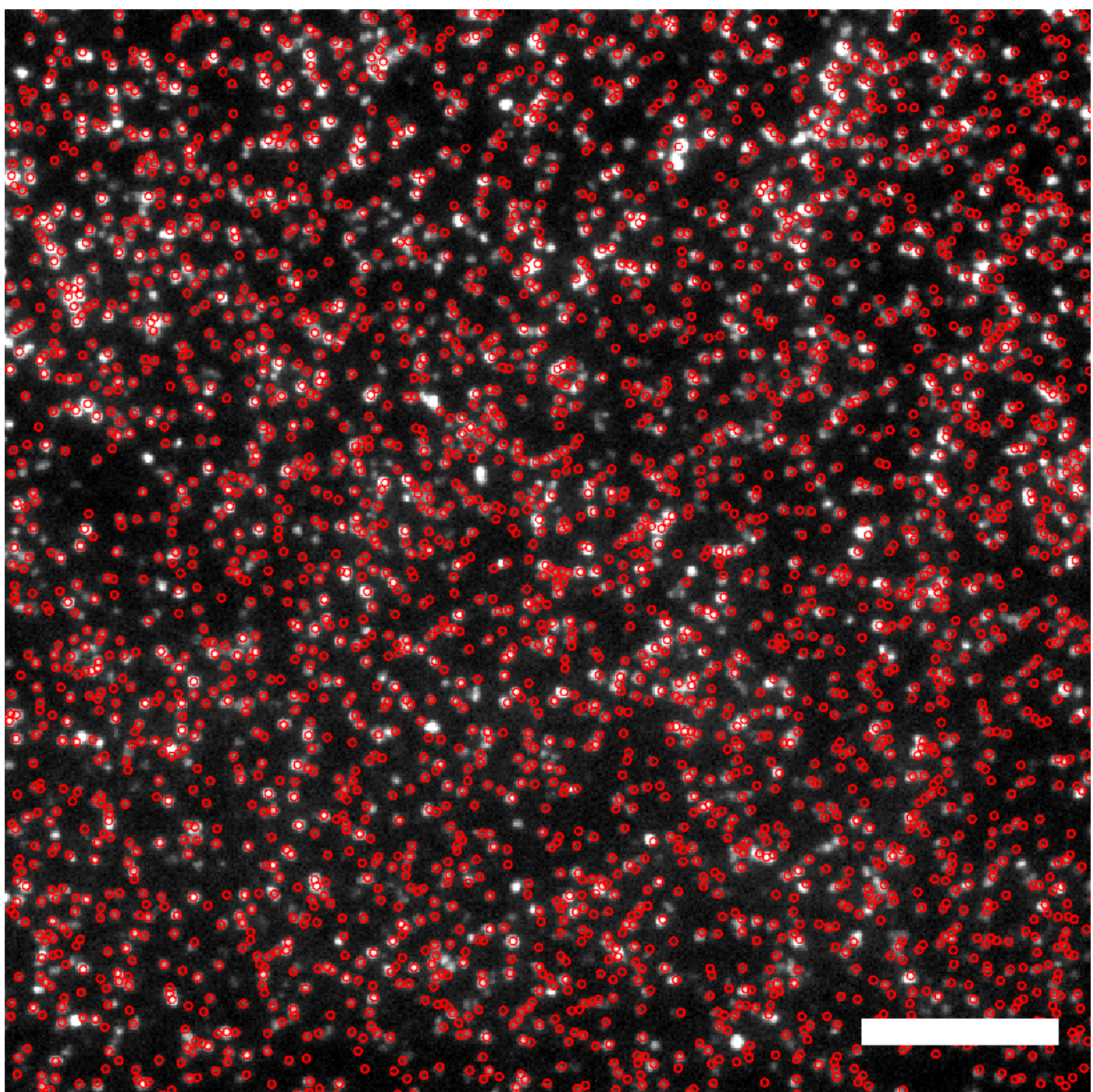


Figure S5 | Identification of activator sequences from the FASTQ data. A representative FOV (512×512 pixel; $110 \times 110 \mu\text{m}^2$) of aligned red NCBs polonies acquired under the red channel (EX/EM: 620/60, 700/75). The library sequences (i.e., activators) are hybridized with the common NC probe (i.e., C55) and form activated NCBs on the chip. The registered activator positions from the FASTQ data file are circled in red. These two examples (Fig. S4 and S5) demonstrate the accuracy of the NCB-CHAMP⁶ mapping algorithm. Scale bar: 20 μm .

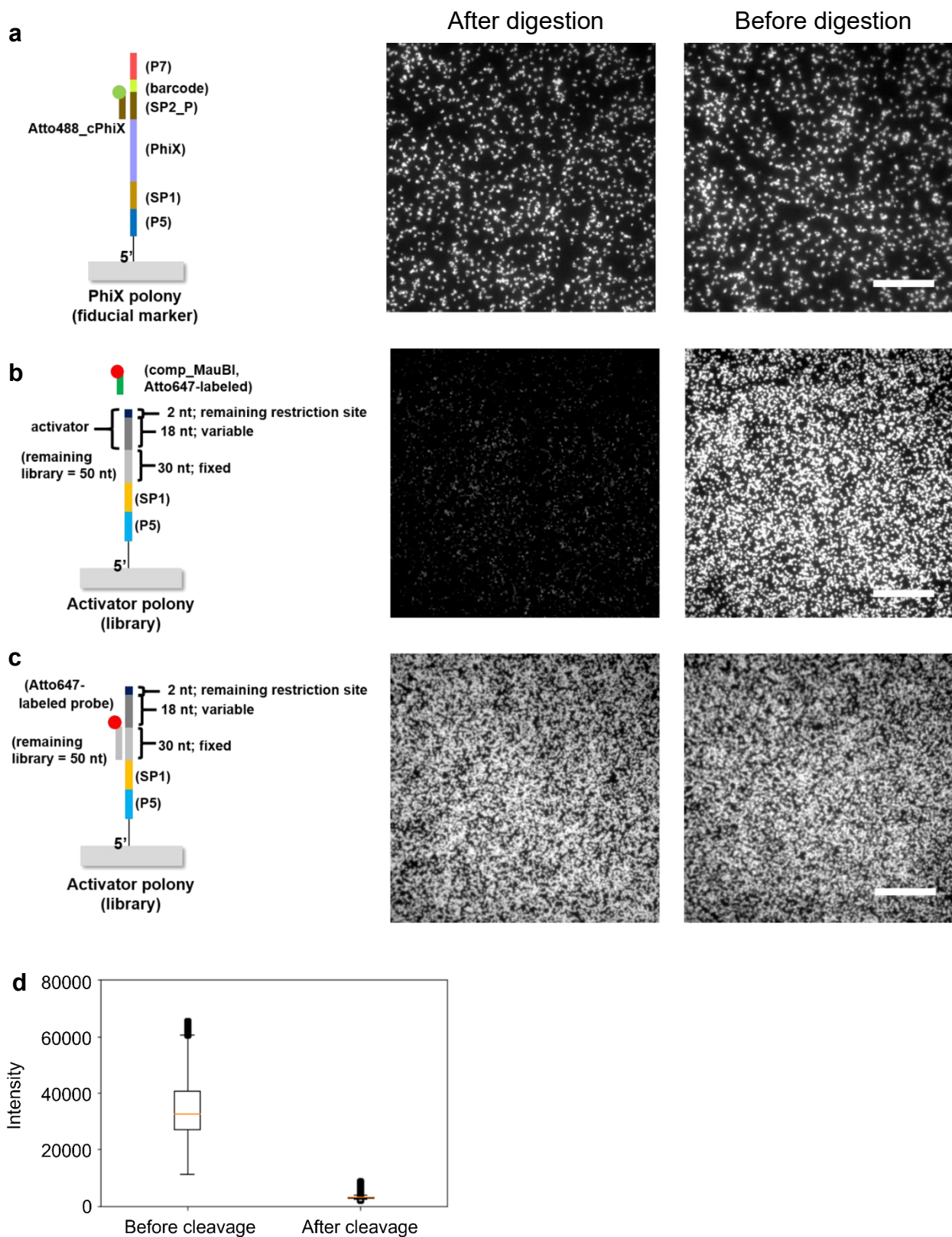


Figure S6 | MiSeq chip images before and after restriction enzyme digestion. **a** PhiX image is unaffected after cleavage. **b** Overhang is successfully cleaved as minimal Atto647N-labeled comp_SP2 probes can still bind with the activator polonies. **c** The library sequences are unaffected after digestion. **d**. We averaged one row of Atto647-tagged fluorescence images. The median intensity dropped ~90% after cleavage. Box plots represented median and 25th and 75th percentiles—interquartile range; IQR—and whiskers extended to 1.5× IQR from the hinges. Empty circles represented the outliers. **b** and **c** panels had the same contrast setting, while the contrast setting of **a** panel was different. Scale bar: 25 μm.

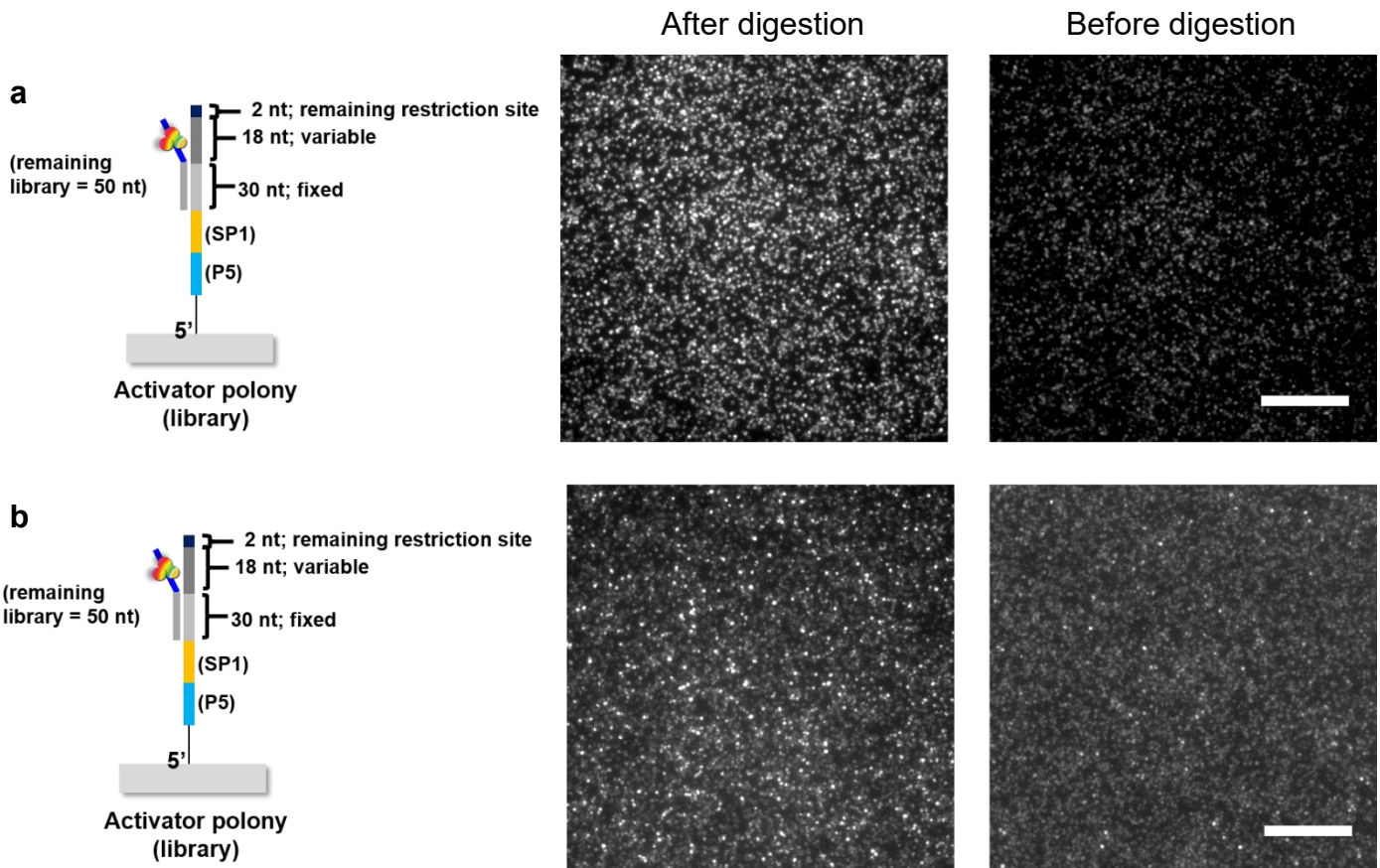


Figure S7 | NCBs images before and after digestion. **a** After restriction enzyme digestion, stronger NCBs signals are observed in the red channel. **b** Stronger NCBs signals are observed in the yellow channel. **a** and **b** panels had the same contrast setting. Scale bar: 25 μ m.

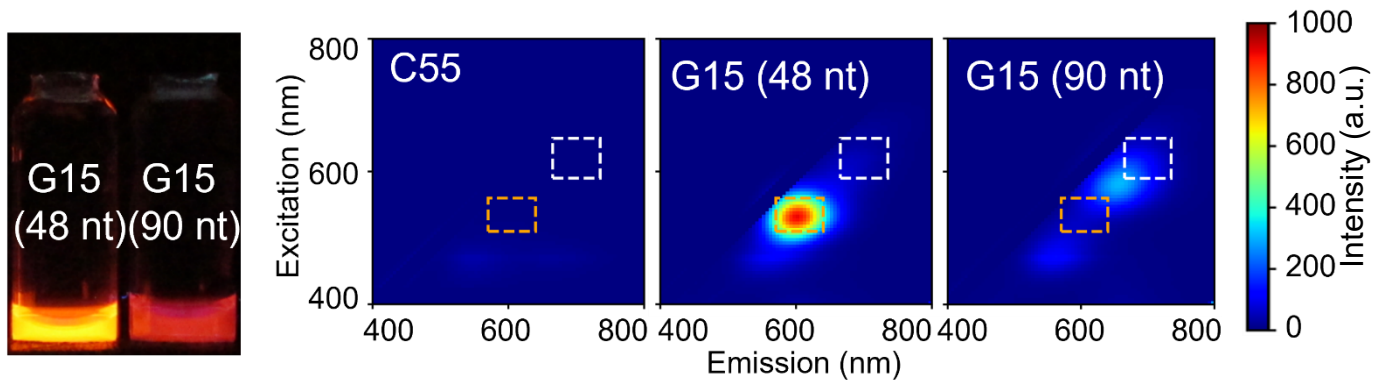


Figure S8 | Illumination comparison of canonical NCBs with different activator length. We observed red-shifted fluorescence for NCBs having longer G15 activator (90-nt long) compared to canonical G15 activator (48-nt long).

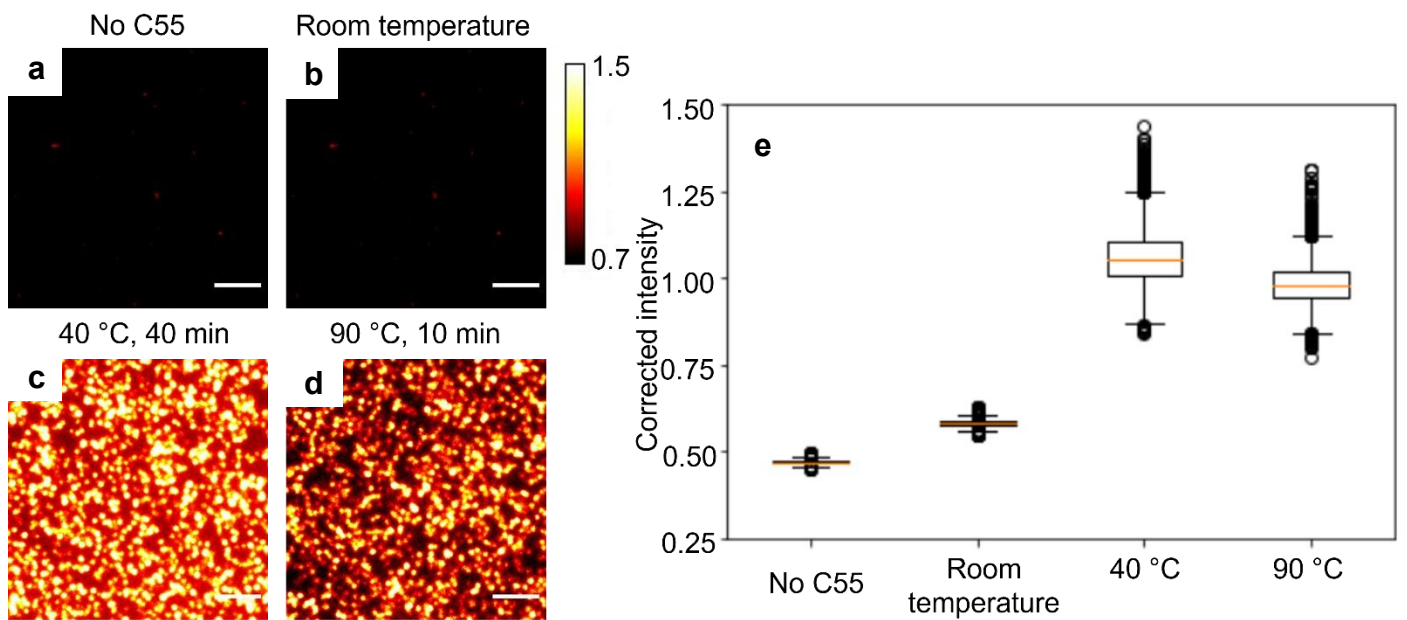
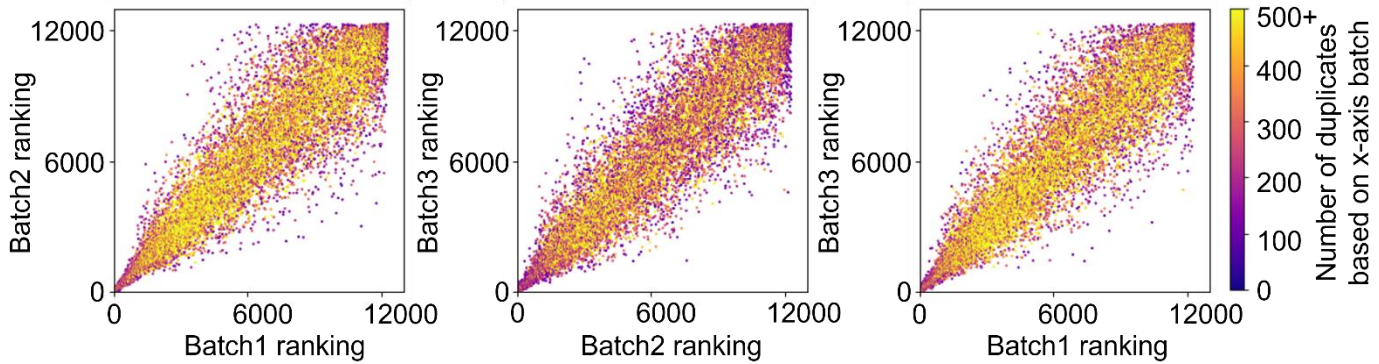
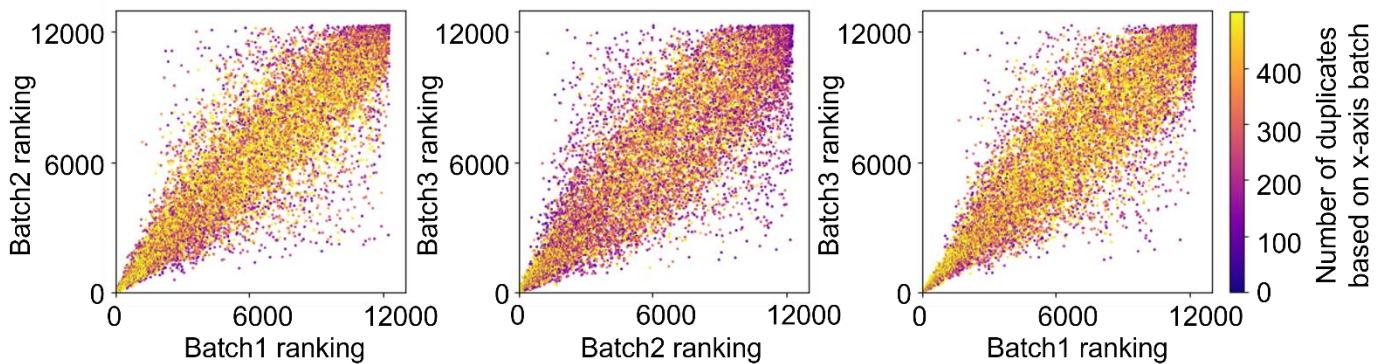


Figure S9 | Intensity comparison of NCBs on the chip under different hybridizing temperature. We tested the NCBs intensity on the chip with different hybridizing temperature. We found that 40 °C gave the brightest mean intensity compared to 90 °C, which was the condition similar as test-tube validation. Furthermore, as 40 °C gave a more moderate condition to the delicate *MiSeq* chip, we applied 40 °C to the chip experiments throughout this report. Box plots represented median and 25th and 75th percentiles—interquartile range; IQR—and whiskers extended to 1.5× IQR from the hinges. Empty circles represented the outliers.

a Library_1 (red):



b Library_1 (yellow):



c Statistics of *MiSeq chip* results for Library_1

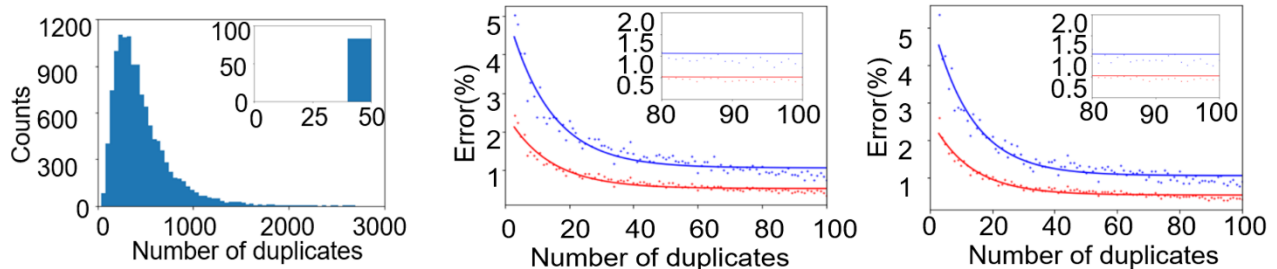
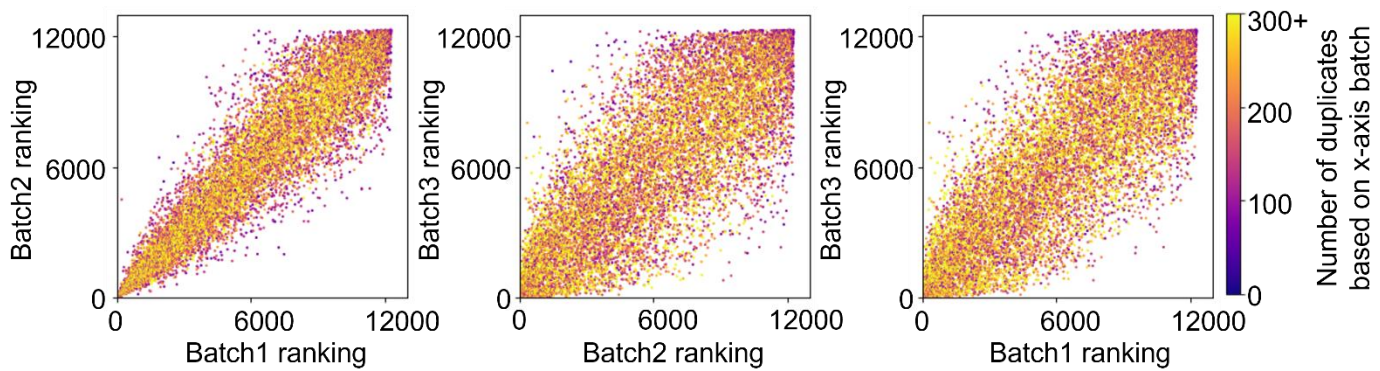


Figure S10 | Batch to batch variations in *MiSeq chip* selection for library_1. Nonparametric measure is applied to evaluate the ranking correlation among repeated experiments. **a** For library_1, all 12,286 distinct sequences are found on chip. The Spearman's rho for the 3 comparisons in red channel are 0.92, 0.93, and 0.93, with the R^2 of 0.85, 0.86 and 0.86 (left to right). **b** The Spearman's rho for the 3 comparisons in yellow channel are 0.86, 0.91, and 0.86, with the R^2 of 0.75, 0.83 and 0.75 (left to right). **c** (left) Distribution of the number of activator duplicates in library_1. All activators had at least 20 duplicates observed. On average, each activator had 457 ± 308 polonies on a *MiSeq* chip. (middle and right) Estimation of error in the NCB brightness characterization after bootstrapping. To improve the accuracy of our high-throughput screening, we performed 100 rounds of bootstrapping processes by random sampling 75% of observed duplicates intensity and assigned median intensity as the NCB on-chip intensity. Bootstrap intensity values were calculated for the standard sequence (i.e., G15) with all numbers of clusters between 3 and 100. Shown are the average errors (red points) and 90% confidence intervals of error (blue points), using the median intensity with either 200 (middle) or 20,000 clusters (right) for 10,000 rounds as reference. Solid lines indicate a fit to the data.

a Library_2 (red):



b Library_3 (red):

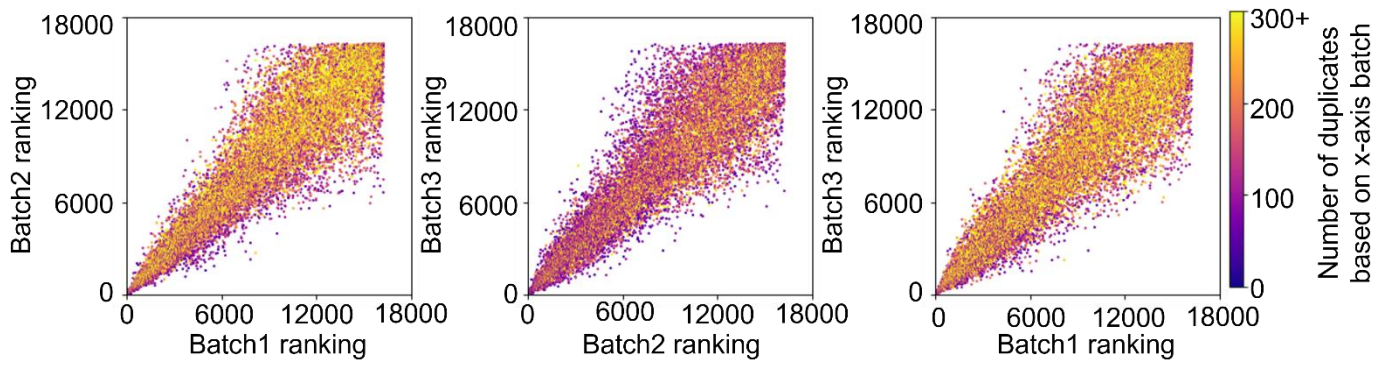


Figure S11 | Batch to batch variations in MiSeq chip selection for library_2 and library_3. **a** For library_2, all 12,286 distinct sequences are found on chip. The Spearman's rho for the 3 comparisons in red channel are 0.93, 0.83 and 0.80 (left to right), with the R^2 of 0.87, 0.68, and 0.65 (left to right). **b** For library_3, all 16,255 distinct sequences are found on chip. The Spearman's rho for the 3 comparisons in red channel are 0.91, 0.86 and 0.89 (left to right), with the R^2 of 0.82, 0.73 and 0.79 (left to right).

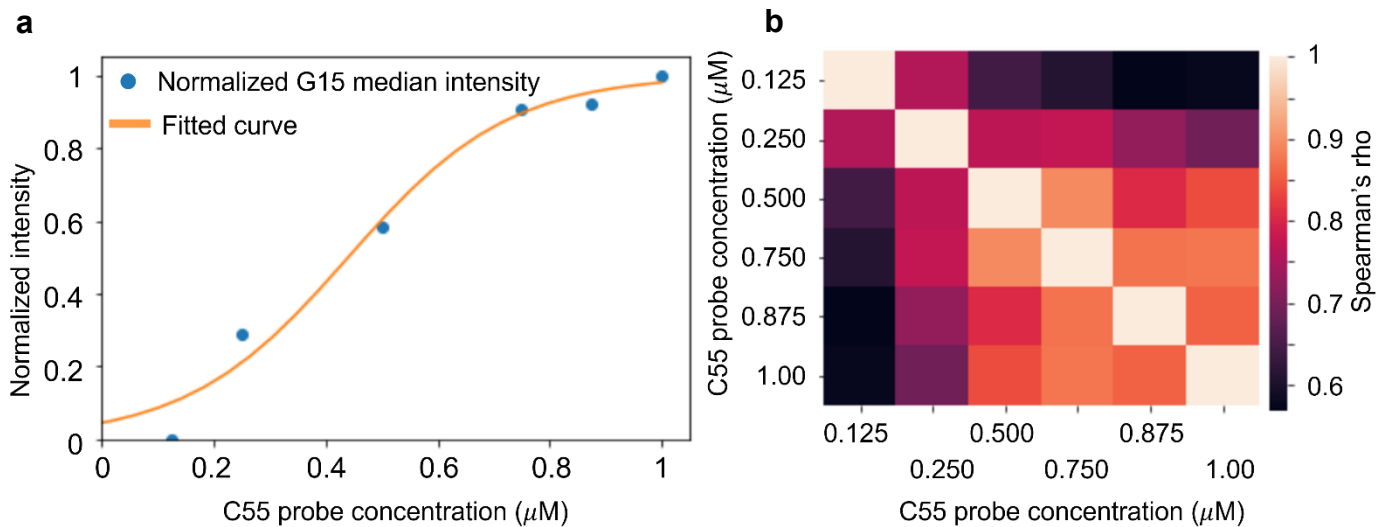


Figure S12 | Titration curve of G15 NCB intensity on the chip. **a** To find out the optimal condition for NCB screening on *MiSeq* chip, we used the G15 NCB intensity as the calibration standard in a titration experiment. C55 probes at 6 different concentrations were delivered to the chip. The normalized G15 NCB intensity reached a plateau when the C55 probe concentration was about 0.8 μM . **b** However, we also observed highly consistent ranking results if C55 probe concentrations were higher than 0.5 μM .

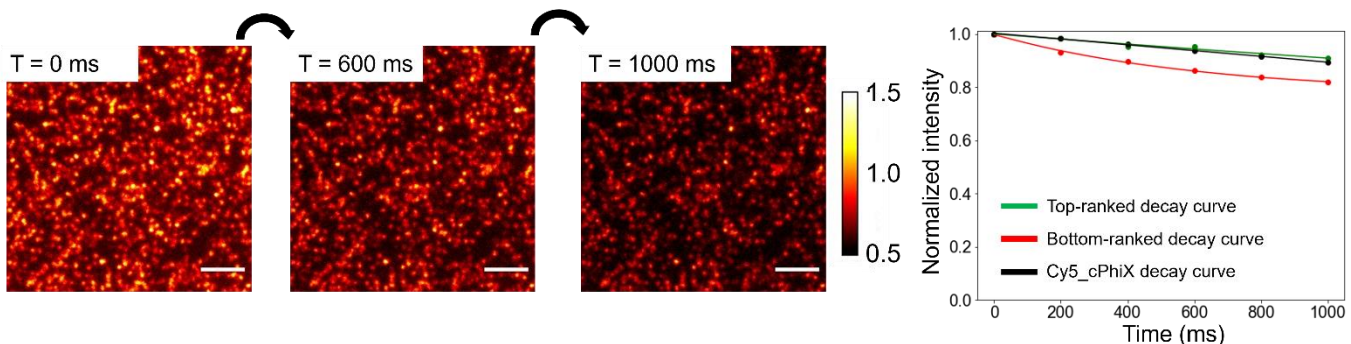
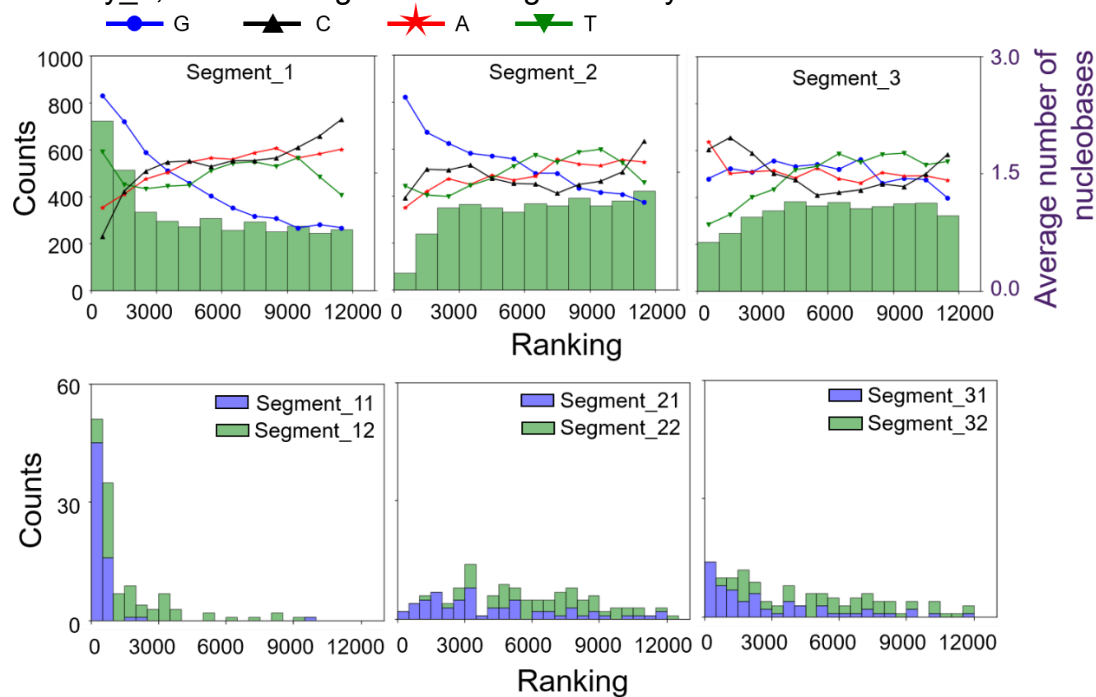
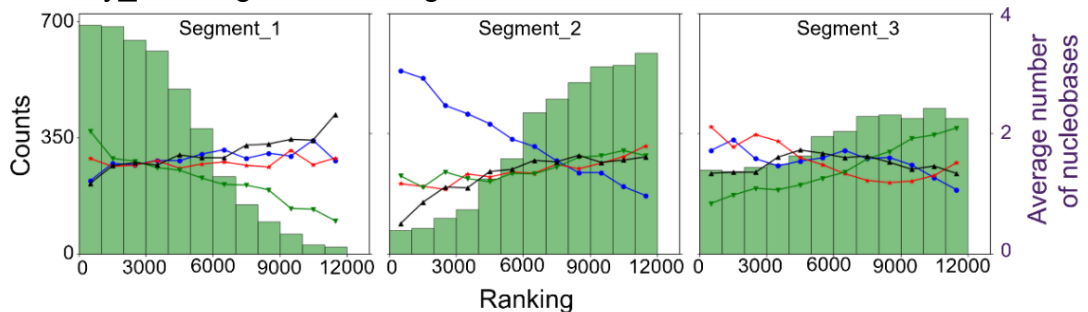


Figure S13 | NCB intensity decay on the chip. By acquiring a fluorescence image every 200 ms, intensity time traces of polonies were obtained, which could be fitted with a single-exponential decay. After one second of strong illumination ($\sim 10 \text{ W/cm}^2$), polony intensity decreased by $\sim 20\%$ at most.

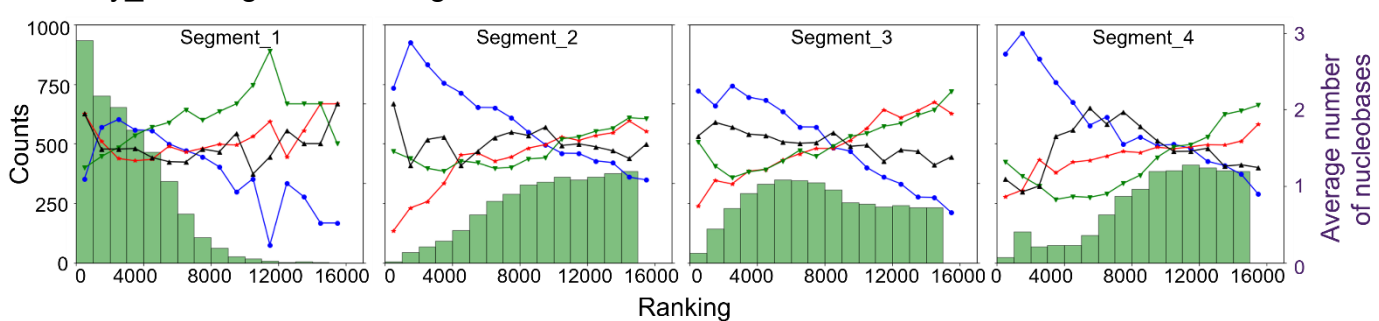
a Library_1, 3- and 6-segment interrogation on yellow NCBs



b Library_2, 3-segment interrogation on red NCBs



c Library_3, 4-segment interrogation on red NCBs



d Detailed explanation of Fig. 2c

Activator1:

ATCCGTGGGGGGGGGG

Activator2:

ACCATTGGGGGGGGGG

Number of adenine = 1

Number of adenine = 2

Number of thymine = 2

Number of thymine = 2

Number of guanine = 1

Number of guanine = 0

Number of cytosine = 2

Number of cytosine = 2

Average number of nucleobases =

$$\left(\frac{\sum_i (\text{number of nucleobases})_{\text{activator } i}}{\text{total number of activators considered}} \right)$$

$$\text{Average number of adenines} = \frac{1+2}{2} = 1.5$$

$$\text{Average number of thymines} = \frac{2+2}{2} = 2$$

$$\text{Average number of guanines} = \frac{1+0}{2} = 0.5$$

$$\text{Average number of cytosines} = \frac{2+2}{2} = 2$$

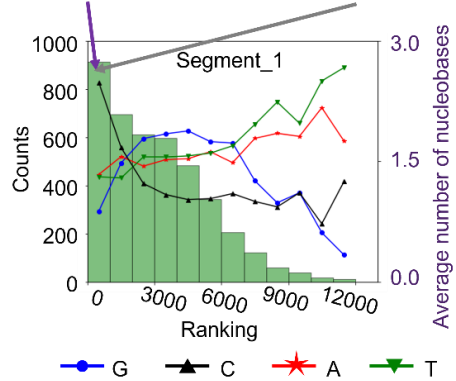


Figure S14 | Influence of activator mutations on NCB brightness. **a** Here we showed the influence of activator mutations on yellow NCB brightness. **b** When randomizing the 3 segments in library_2, positions 10 to 15 were found to be the interaction hot zone. The segment definition for all three libraries could be found in **Table S1c**. **c** When randomizing the 4 segments in library_3, positions 10 to 12 were found to be the interaction hot zone. The results from **(b)** and **(c)** were consistent with the library_1 result (**Fig. 2**), which showed positions 10-12 were the interaction hot zone for creating bright NCBs. **d** Here we demonstrated calculation of the average number of nucleobases from two top-ranked sequences. For instance, Activator1 (Left, ATCCGT GGTGGG GTGGGG, rank no.12) has 1 adenine, 2 thymine, 1 guanine, and 2 cytosine, while the Activator2 (Right, ATCCGT GGTGGG GTGGGG, rank no. 14) has 2 adenine, 2 thymine, 0 guanine, and 2 cytosine. Both activators were highly ranked (i.e., they create bright NCBs) and located in the first bin (ranking 1-1,000) of the histogram. Each histogram contained 4,096 sequences.

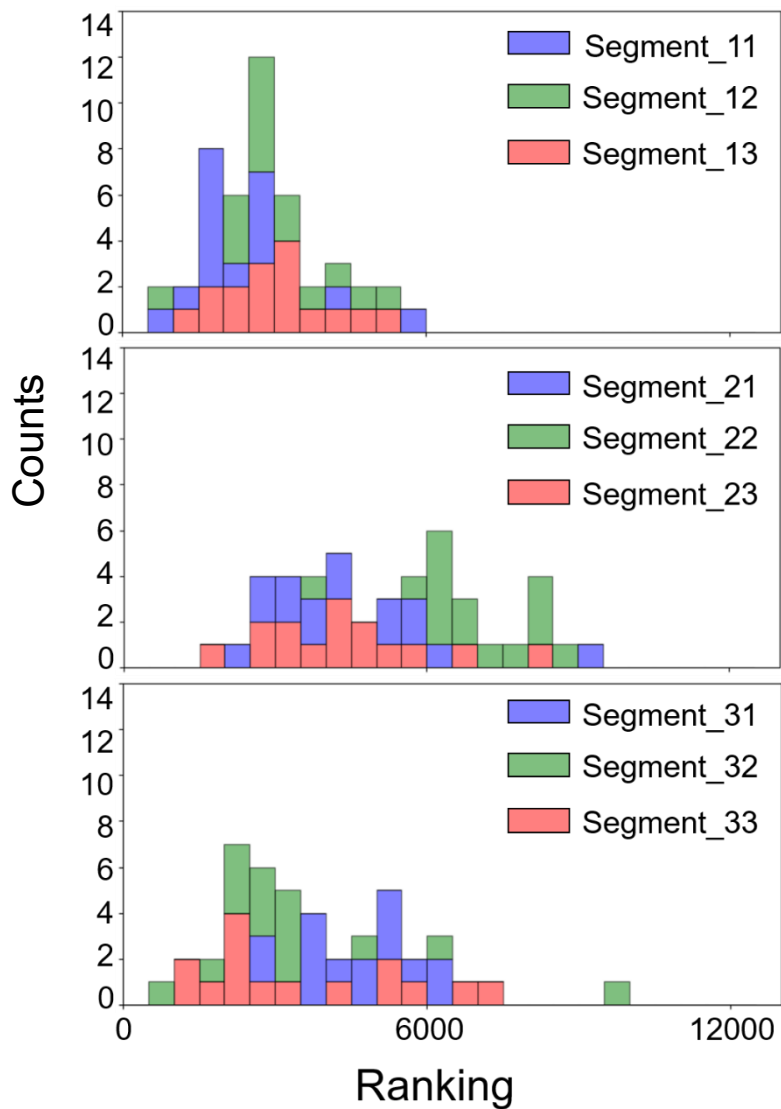
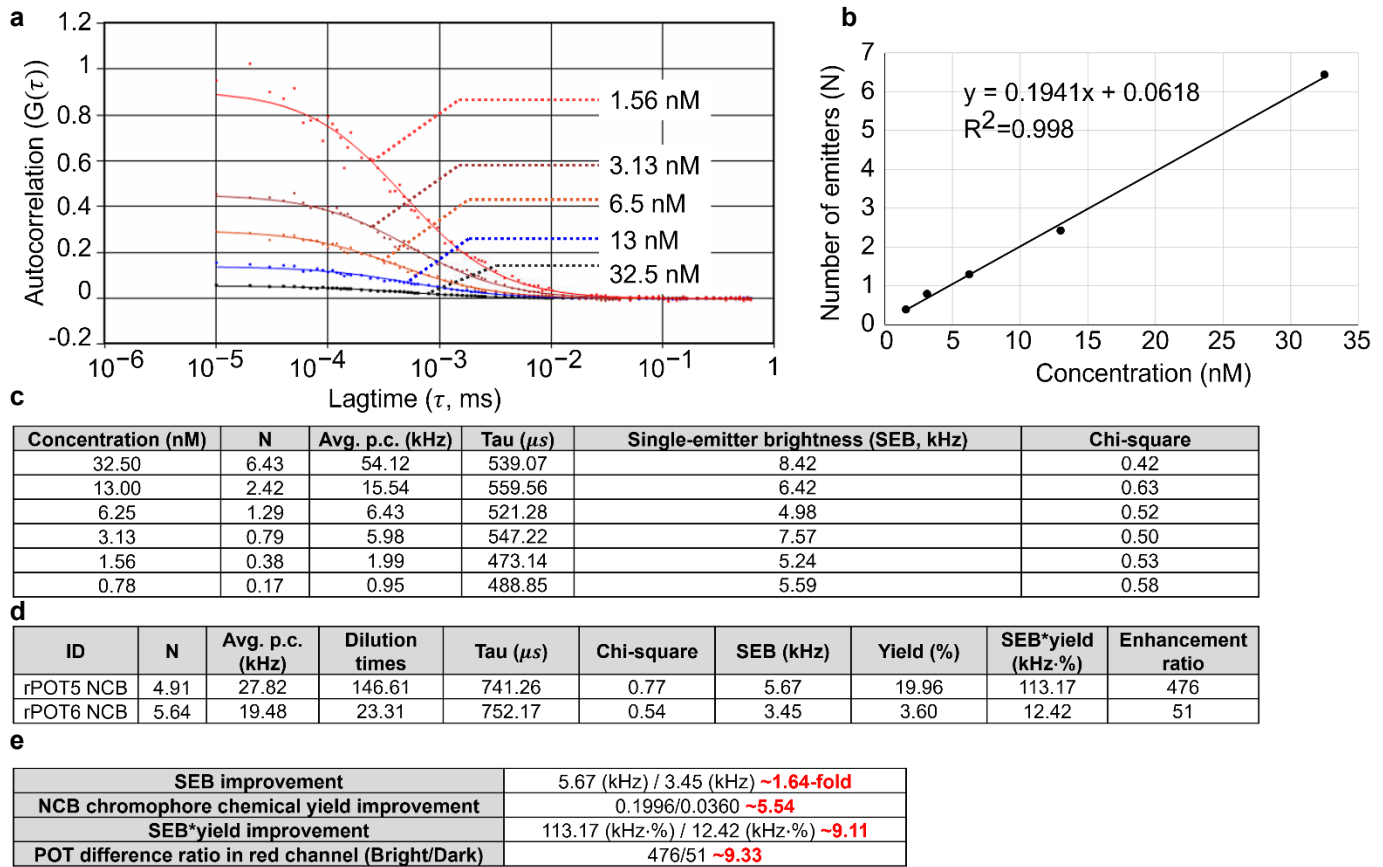


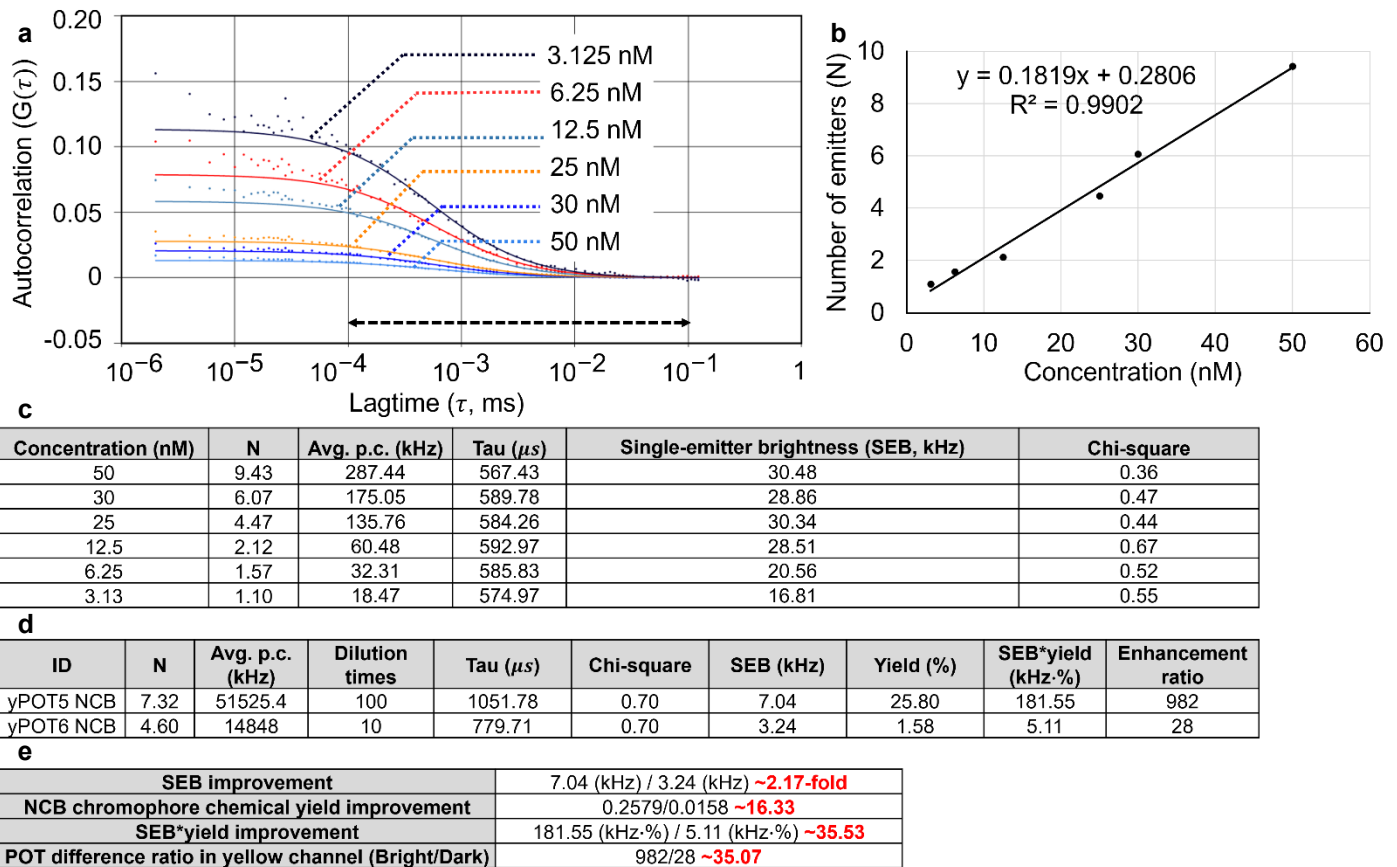
Figure S15 | Nine-segment interrogation on the library_1 for red NCB brightness. Here we further divide the library_1 activator into 9 segments (**Table S1b**) and investigate each segment's influence on red NCBs brightness. In segment_2, segment_22 (positons 9-10) and segment_23 (positions 11-12) are the critical zones as the ranking shifts toward the dark side when these segments are randomized.



Avg. p. c. (average photon count); N (number of emitters in detection volume);

Tau (dwell time of emitters in detection volume); SEB (single-emitter brightness)

Figure S16 | Fluorescence correlation spectroscopy (FCS) results on the red NCBs. **a** The amplitude of autocorrelation function, $G(0)$, is inversely proportional to the fluorophore concentration (Atto647N-labeled ssDNA, for calibration purpose), demonstrating no optical saturation in our FCS experiments. **b** Number of emitters in the detection volume ($1/G(0)$) shows a linear relationship with the emitter concentration, generating a calibration curve. **c** The fitting parameters of the calibration FCS experiment on Atto647N-labeled ssDNA. **d** The fitting parameters of the FCS experiment on rPOT5 and rPOT6 NCBs, which are an extreme POT (Fig. 3). **e** From the FCS experiment, it is clearly to see that a single rPOT5 emitter is 1.64-fold brighter than a single rPOT6 emitter (which we term “single-emitter brightness”, SEB), and the concentration of rPOT5 emitter is 5.54 higher than that of rPOT6 emitter (which we call “chromophore chemical yield” or “yield” – not all NC probes carry a AgNC that can be activated). The product of SEB improvement and chromophore chemical yield improvement (9.11) is about the same as the improvement in ensemble enhancement ratio identified by the fluorometer (9.33), indicating that the intensity difference seen in rPOT NCBs is a result of different yield and different SEB. For FCS setup and analysis, please refer to **Methods**.



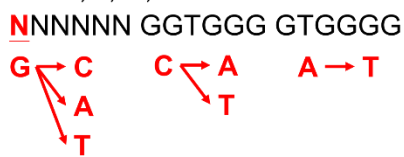
Avg. p. c. (average photon count); N (number of emitters in detection volume);

Tau (dwell time of emitters in detection volume); SEB (single-emitter brightness)

Figure S17 | Fluorescence correlation spectroscopy (FCS) results on the yellow NCBs. **a** The amplitude of autocorrelation function, $G(0)$, is inversely proportional to the fluorophore concentration (Atto532N-labeled ssDNA, for calibration purpose), demonstrating no optical saturation in our FCS experiments. **b** Number of emitters in the detection volume ($1/G(0)$) shows a linear relationship with the emitter concentration, generating a calibration curve. **c** The fitting parameters of the calibration FCS experiment on Atto532N-labeled ssDNA. **d** The fitting parameters of the FCS experiment on yPOT5 and yPOT6 NCBs, which are an extreme POT (Fig. 3). **e** From the FCS experiment, it is clearly to see that the SEB of yPOT5 emitter is 2.17-fold brighter than that of yPOT6 emitter, and the chromophore chemical yield of yPOT5 emitter is 16.33 higher than that of yPOT6 emitter. The product of SEB improvement and chromophore chemical yield improvement (35.53) is about the same as the improvement in ensemble enhancement ratio identified by the fluorometer (35.07), indicating that the intensity difference seen in yPOT NCBs is a result of different yield and different SEB. For FCS setup and analysis, please refer to **Methods**.

a

$N = A, T, C, G$



For each segment, the number of twin NCB pairs would be,

$$6 \times 4^5 = 36,864$$

Total number of twin NCB pairs would be,

$$3 \times 36864 = 110,592$$

1. GGGTGGGGTGGGGTGGGG vs. CGGTGGGGTGGGGTGGGG
2. GGGTGGGGTGGGGTGGGG vs. AGGTGGGGTGGGGTGGGG
3. GGGTGGGGTGGGGTGGGG vs. TGGTGGGGTGGGGTGGGG
4. CGGTGGGGTGGGGTGGGG vs. AGGTGGGGTGGGGTGGGG
5. CGGTGGGGTGGGGTGGGG vs. TGGTGGGGTGGGGTGGGG
6. AGGTGGGGTGGGGTGGGG vs. TGGTGGGGTGGGGTGGGG

6 pairs of twin NCBs could be generated from 3 activators, GGGTGGGGTGGGGTGGGG, CGGTGGGGTGGGGTGGGG, AGGTGGGGTGGGGTGGGG

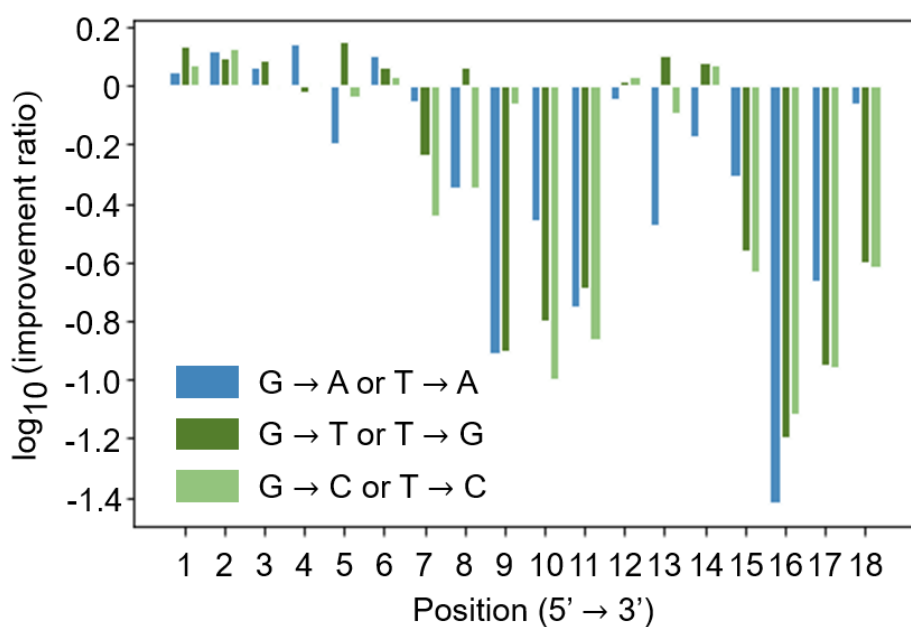
b

Figure S18 | Calculation for the number of twin NCB pairs in library_1 and small-scale test-tube investigation of G15 twin NCBs in the yellow channel. **a** Although library_1 only has 12,286 activators, they give us totally 110,592 twin NCB pairs. For each position in segment_1, there are 6 scenarios for creating twin NCBs at that position. Considering we have 6 positions in segment_1 and we fill up the rest of the 5 positions using the 4^5 combinations, we have $6 \times 4^5 \times 6 = 36,864$ distinct twin NCB pairs just for segment_1. For 3 segments, there are totally $3 \times 36,864 = 110,592$ distinct twin NCB pairs in library_1. **b** The improvement ratios of 54 G15 twin NCBs are put into this base-10 logarithm chart. By substituting G to T at position 5 (i.e., GGGTTGGGTGGGGTGGGG), the largest improvement in the enhancement ratio is observed, which is only 1.41-fold higher than the enhancement ratio of G15 NCB in the yellow channel. This result demonstrates that a small-scale investigation cannot improve the brightness of an existing NCB by more than 2-fold. Interestingly, by substituting G to A at position 16 (i.e., GGGTGGGGTGGGGTAGG), we observed a pair of POTs with POT difference ratio ~25.

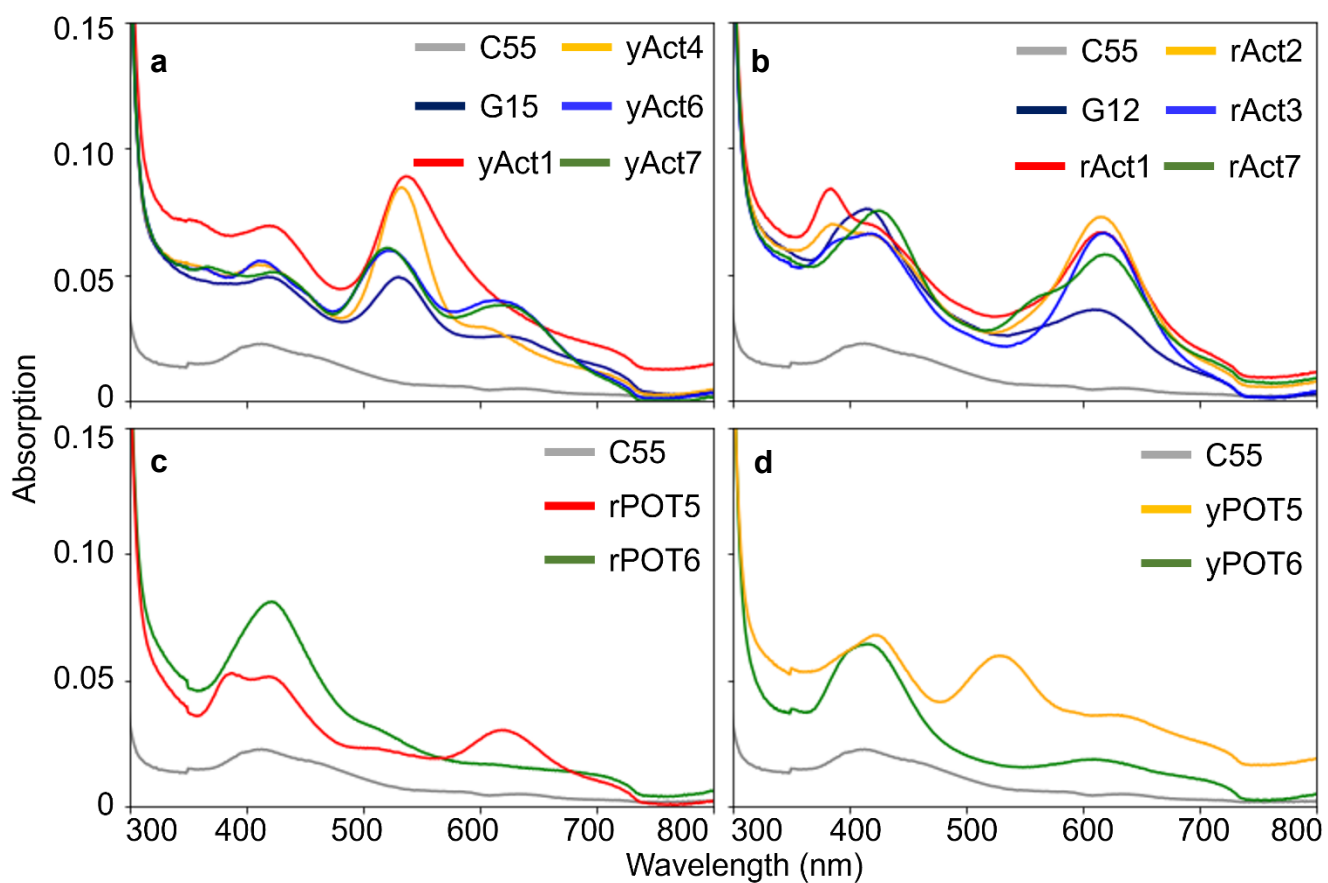


Figure S19 | Absorption spectra of selected NCBs and POTs. **a** For the 5 selected yellow NCBs, we observed the highest absorbance (0.089) for yAct1 NCB at 535 nm, while that of the 5 selected red NCBs reached 0.073 at 610 nm for rAct2 as shown in **(b)**. **c** For rPOT5 and rPOT6 NCBs, differences in their absorption spectra around 610 nm were observed (0.030 for rPOT5 and 0.017 for rPOT6). **d** For yPOT5 and yPOT6 NCBs, differences in their absorption spectra around 530 nm were observed (0.060 for yPOT5 and 0.015 for yPOT6).

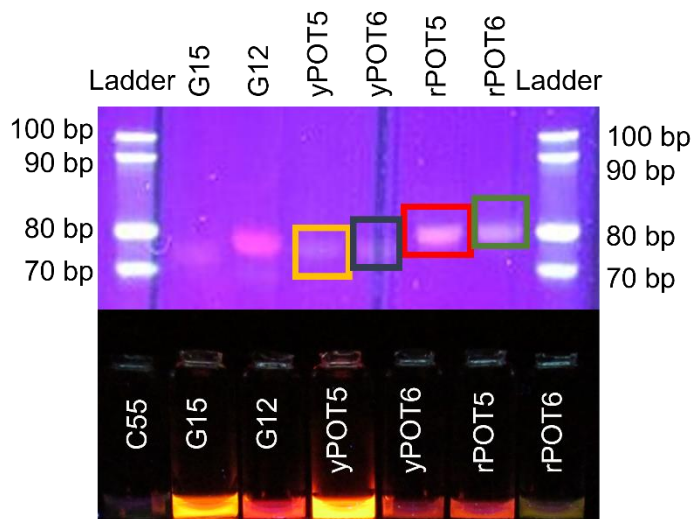
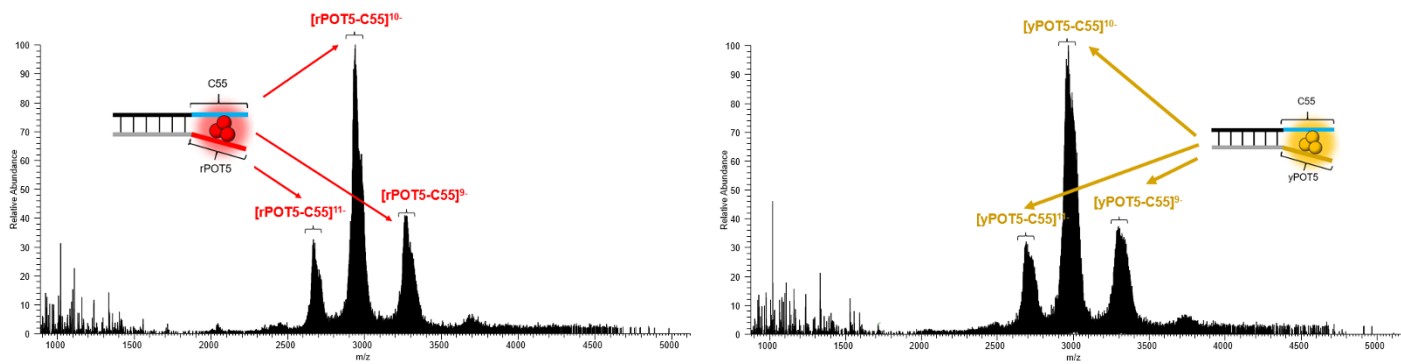


Figure S20 | Native PAGE gel photo under UV excitation. We assessed the mobility of selected NCBs using 20% native PAGE gel. Four of the NCBs (yPOT5, yPOT6, rPOT5 and rPOT6, highlighted by color boxes) were selected to process purification and ESI-MS analysis afterward.

a 10mM Ammonium acetate



b 10mM Ammonium acetate + 0.1% octylamine

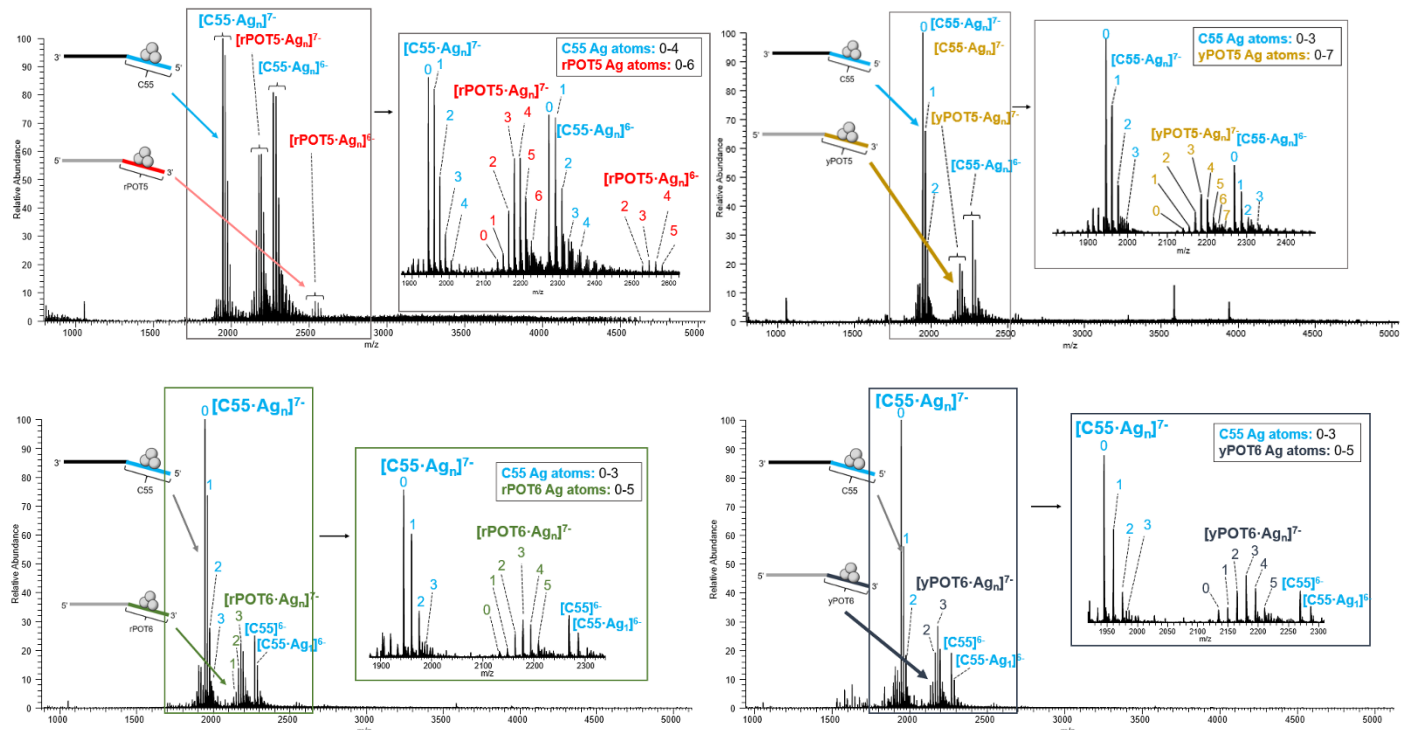


Figure S21 | ESI-MS analysis of selective NCBs. **a** Following the purification using gel electrophoresis, several NCB samples (yPOT5-C55, rPOT5-C55, yPOT6-C55 and rPOT6-C55) were desalting and buffer exchanged into 10 mM ammonium acetate. The resultant mixture was then analyzed by ESI-MS to evaluate the silver stoichiometry of the NCB complexes. **b** Octylamine was added to aliquots of yPOT5-C55 and rPOT5-C55 NCBs (upper row), yPOT6-C55 and rPOT6-C55 (bottom row) at a concentration of 0.1% (v/v), in attempt to reduce the extensive cationic metal adduction that is commonly seen for ESI-MS analysis of oligonucleotides > 20 nt⁴⁰⁻⁴³. Although the addition of octylamine disassembles the NCB complexes into their respective NC probe and an activator sequence, we found the C55 NC probes from the yPOT5 NCB carry 0-4 and the others carry 0-3 silver atoms, while the activators from yPOT5, rPOT5, yPOT6 and rPOT6 NCBs carry 0-7, 0-6, 0-5 and 0-5 silver atoms, respectively. These results indicate that the original silver stoichiometry for the intact yPOT5 NCB may be larger than that of the intact rPOT5 NCB. Moreover, the bright member of POTs may be larger than its counterpart.

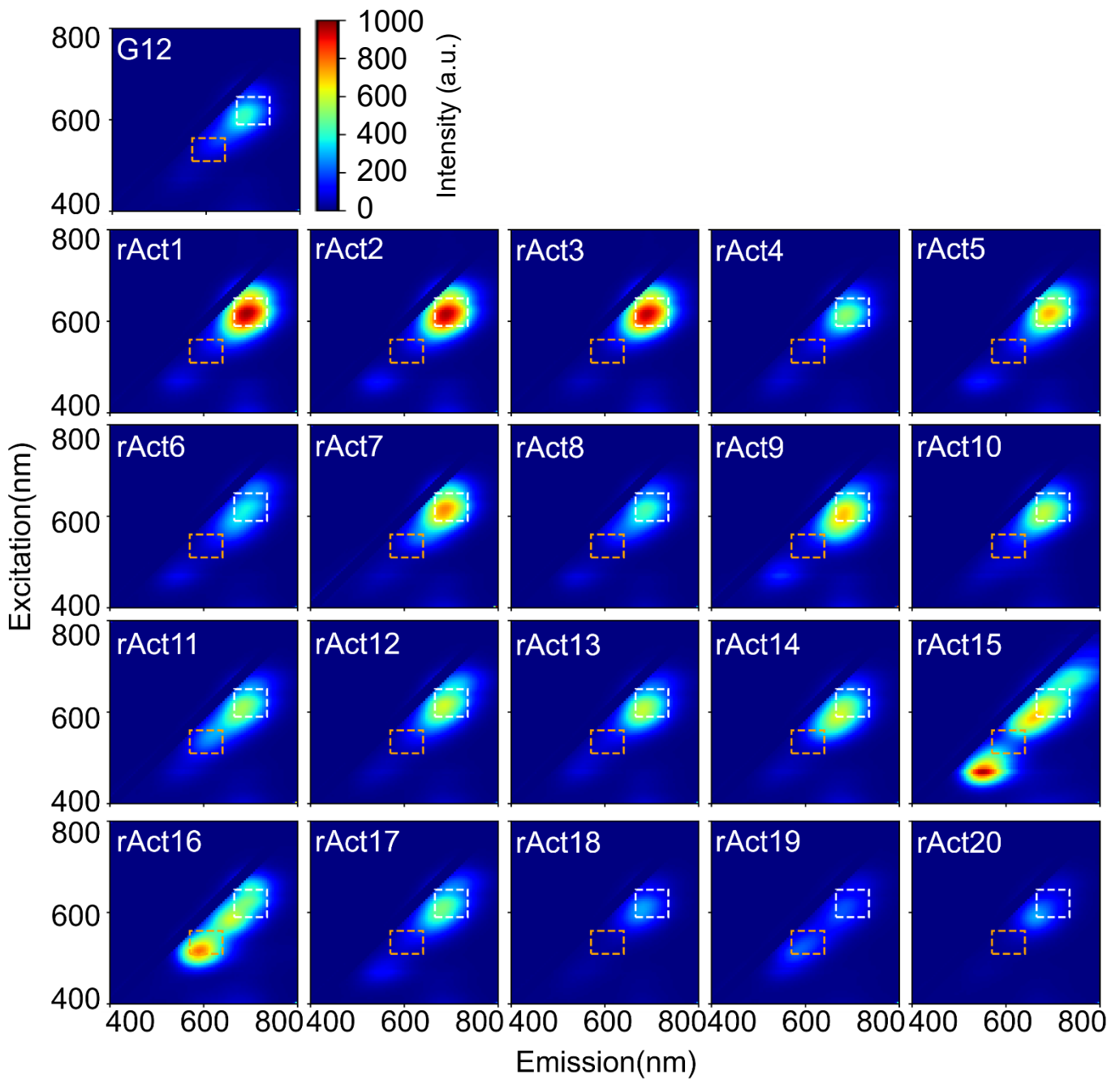


Figure S22 | 2D spectra of bright red activator candidates (including the 3 false positive selections: rACT18, rACT19 and rACT20) Compared to G12 NCB (ATCCGGGGTGGGGTGGGG), 17 out of 20 bright red activator candidates (selected by the chip screening method) have the improvement ratio greater than one (85% accuracy). In particular, rAct1 NCB (TCCATTGGTGGGGTGGGG) has the improvement ratio of 2.94. The white dashed box represents the integrated region of red channel (Ex/Em: 620/60, 700/75 nm), and the orange dashed box represents the integrated region of yellow channel (Ex/Em: 535/50, 605/70 nm). See **Table S2a** for details.

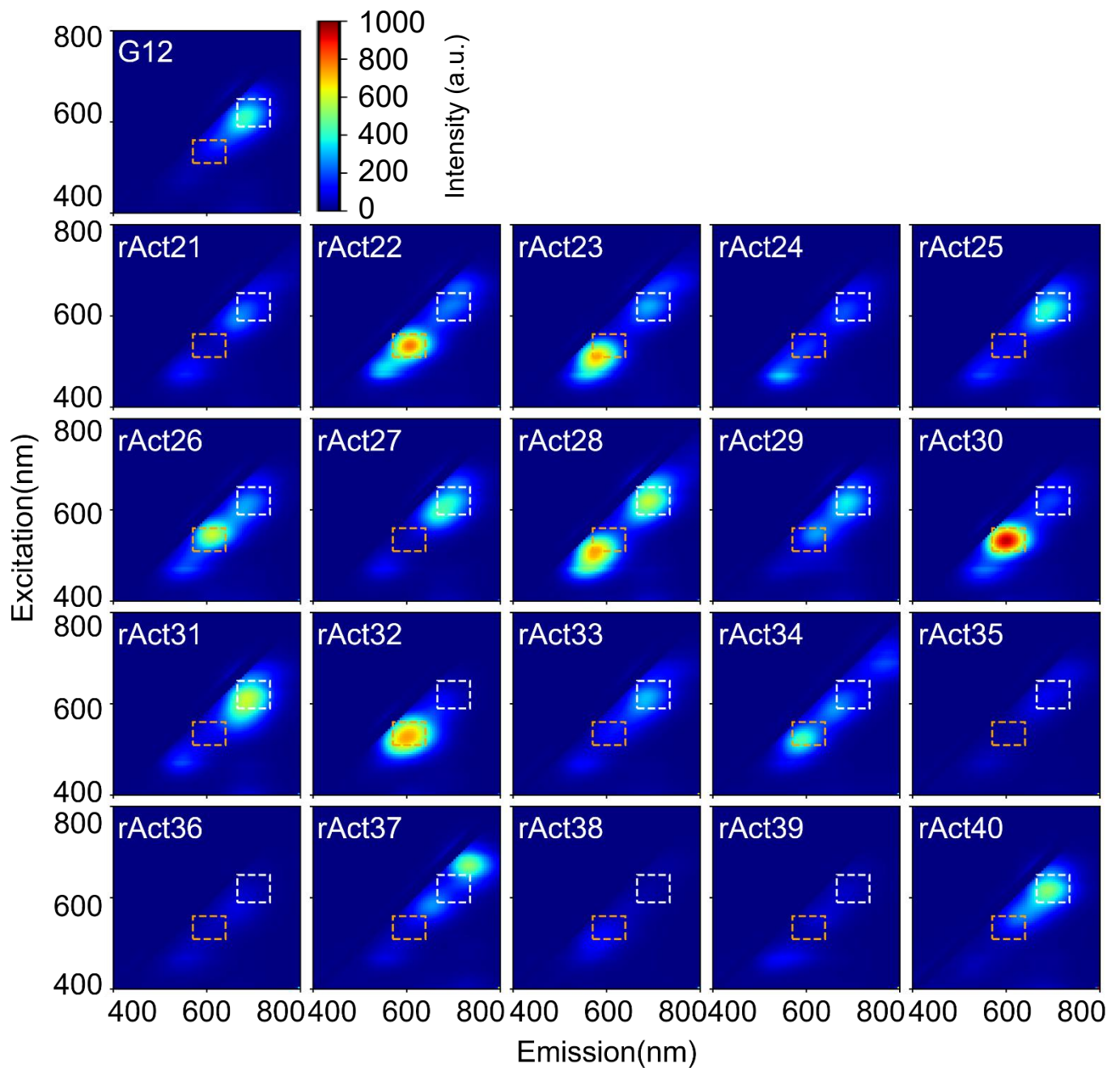


Figure S23 | 2D spectra of dark activator candidates (including 3 false negative selections: rACT28, rACT31 and rACT40) Compared to G12 NCB (ATCCGGGGTGGGGTGGGG), 17 out of 20 dark candidates (selected by the chip screening method) have the improvement ratio less than one (85% accuracy). In particular, rAct38 NCB (GGGTGGGTTATGTGGGG) has the improvement ratio of 0.10. The white dashed box represents the integrated region of red channel (Ex/Em: 620/60, 700/75 nm), and the orange dashed box represents the integrated region of yellow channel (Ex/Em: 535/50, 605/70 nm). See **Table S2b** for details.

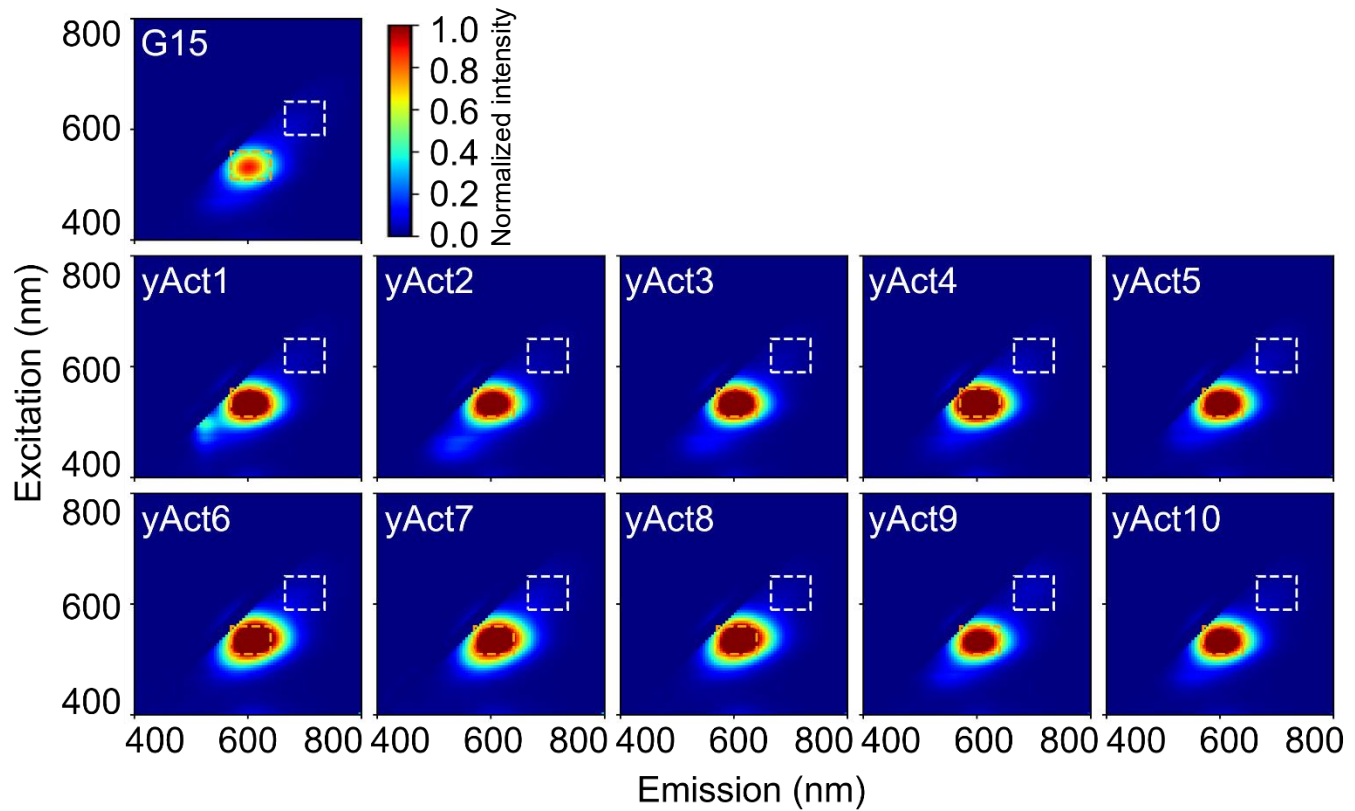


Figure S24 | 2D spectra of bright yellow activator candidates. Compared to G15 NCB (GGGTGGGGTGGGGTGGGG), all 10 bright yellow activator candidates (selected by the chip screening method) have the improvement ratio greater than one (100% accuracy). In particular, yAct4 NCB (TTGGTGGGTGGGGTGGGG) has the improvement ratio of 2.03. Fluorescence intensity normalized to G15 peak intensity. The white dashed box represents the integrated region of red channel (Ex/Em: 620/60, 700/75 nm), and the orange dashed box represents the integrated region of yellow channel (Ex/Em: 535/50, 605/70 nm). See **Table S3** for details.

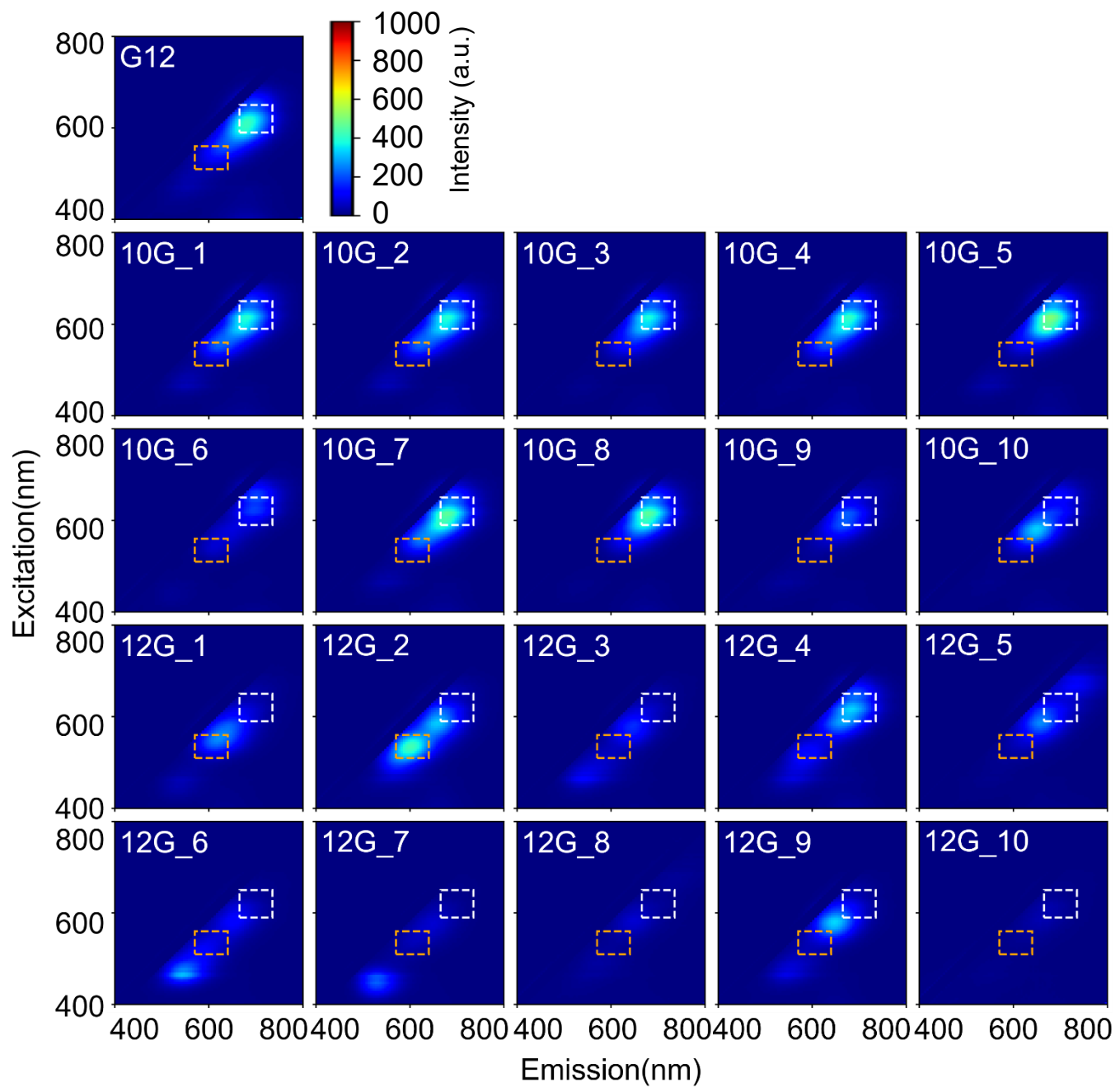


Figure S25 | 2D spectra of activators with various numbers of guanine bases. Based on chip selection results, ten 10G activators can potentially be brighter than G12 NCB (**Table S4**) and ten 12G activators can potentially be darker than G12 NCB (**Table S5**). Test-tube investigation proves that 7 of the selected 10G activators have their enhancement ratios comparable to that of G12 in the red channel (improvement ratio ≥ 0.9). and all selected 12G activators are darker than G12 in the red channel (improvement ratio < 0.6). This result indicates that it is possible to create bright red NCBs with fewer numbers of guanine. The white dashed box represents the integrated region of red channel (Ex/Em: 620/60, 700/75 nm), and the orange dashed box represents the integrated region of yellow channel (Ex/Em: 535/50, 605/70 nm).

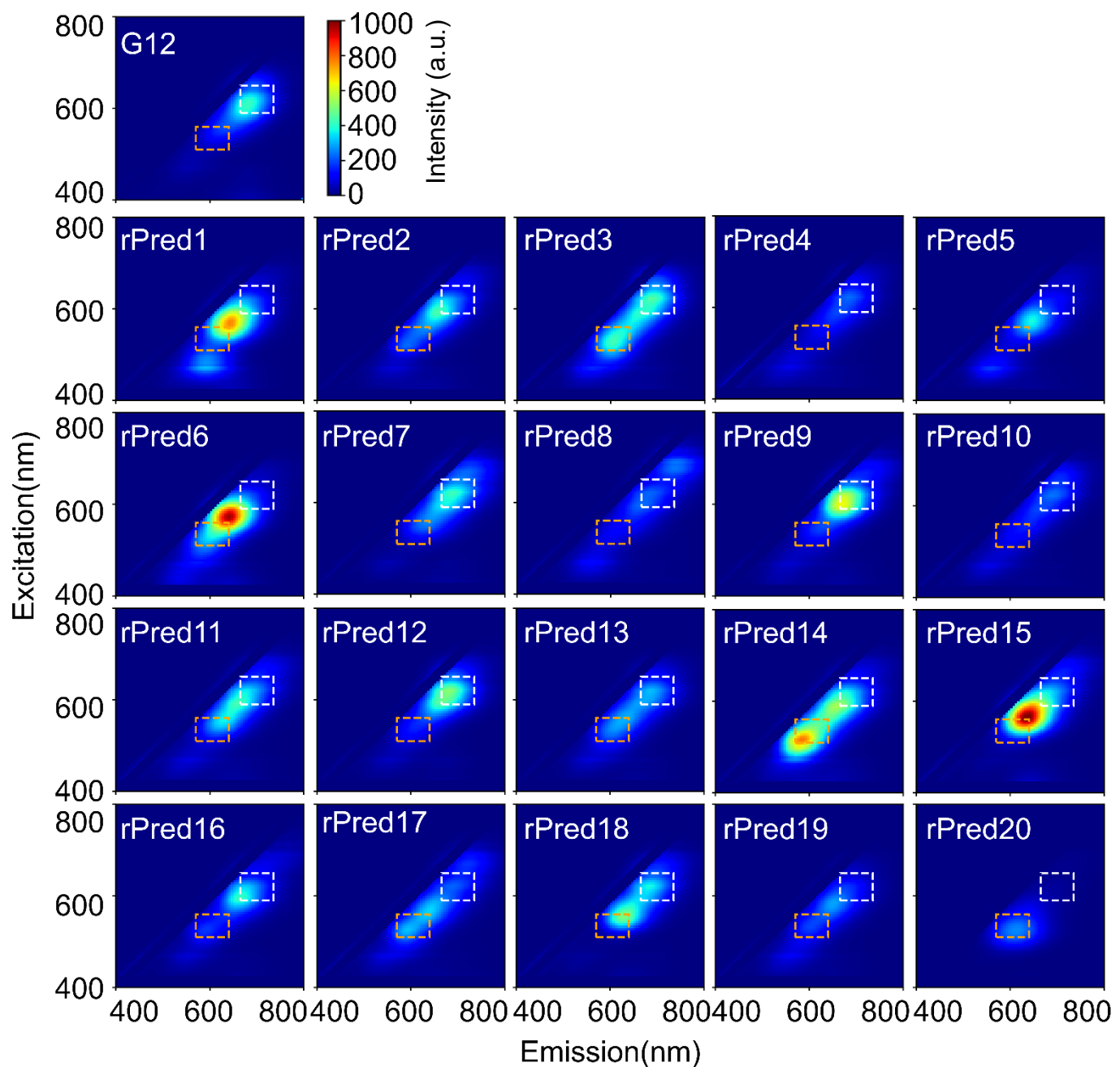


Figure S26 | 2D spectra of rationally designed red NCBs. Twenty activators are designed based on the machine learning results and evaluated in test tubes. On average, the enhancement ratio was 291 for these twenty designs. The white dashed box represents the integrated region of red channel (Ex/Em: 620/60, 700/75 nm), and the orange dashed box represents the integrated region of yellow channel (Ex/Em: 535/50, 605/70 nm).

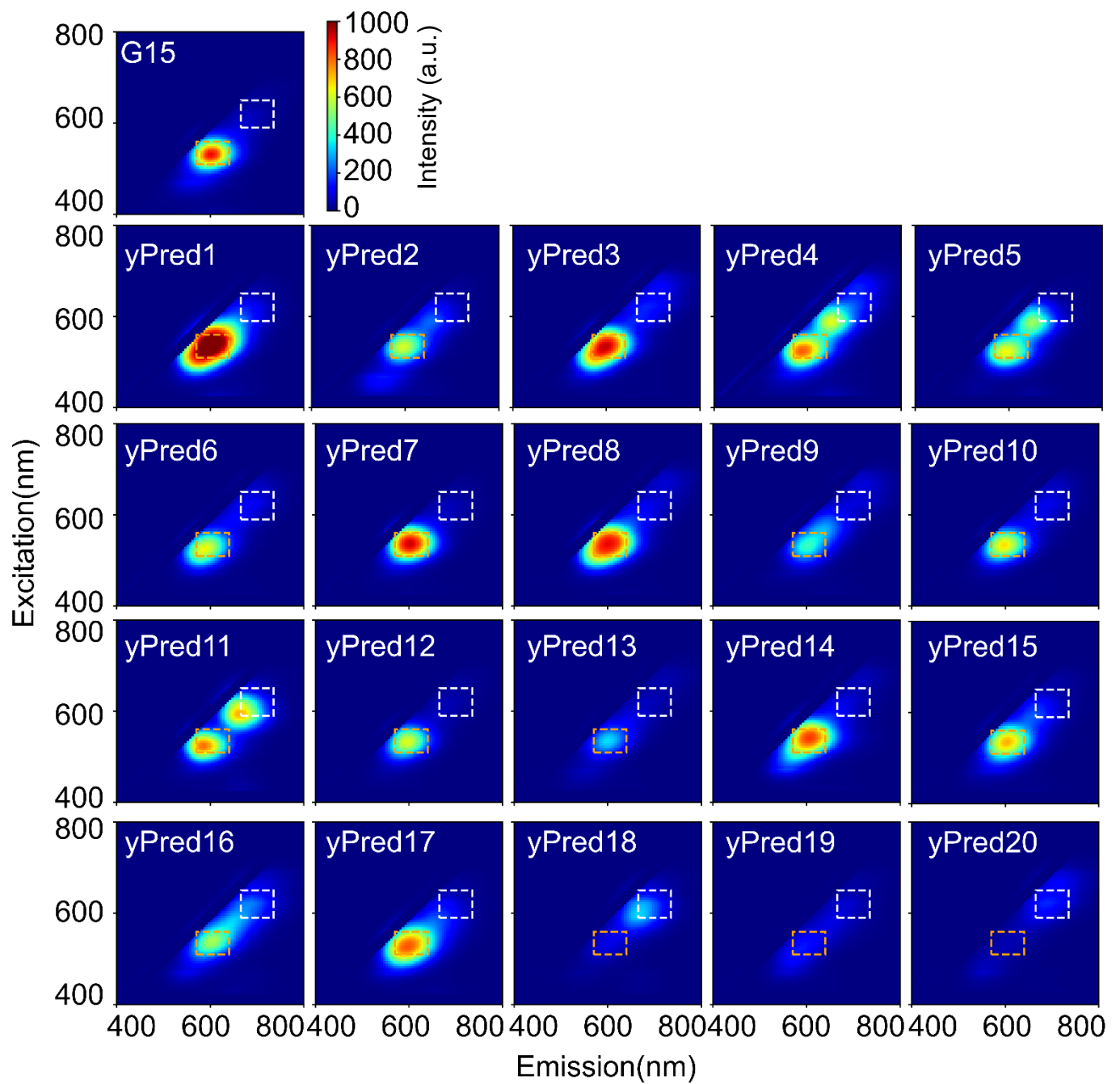


Figure S27 | 2D spectra of rationally designed yellow NCBs. Twenty activators are designed based on the machine learning results and evaluated in test tubes. On average, the enhancement ratio was 532 for these twenty. The white dashed box represents the integrated region of red channel (Ex/Em: 620/60, 700/75 nm), and the orange dashed box represents the integrated region of yellow channel (Ex/Em: 535/50, 605/70 nm).

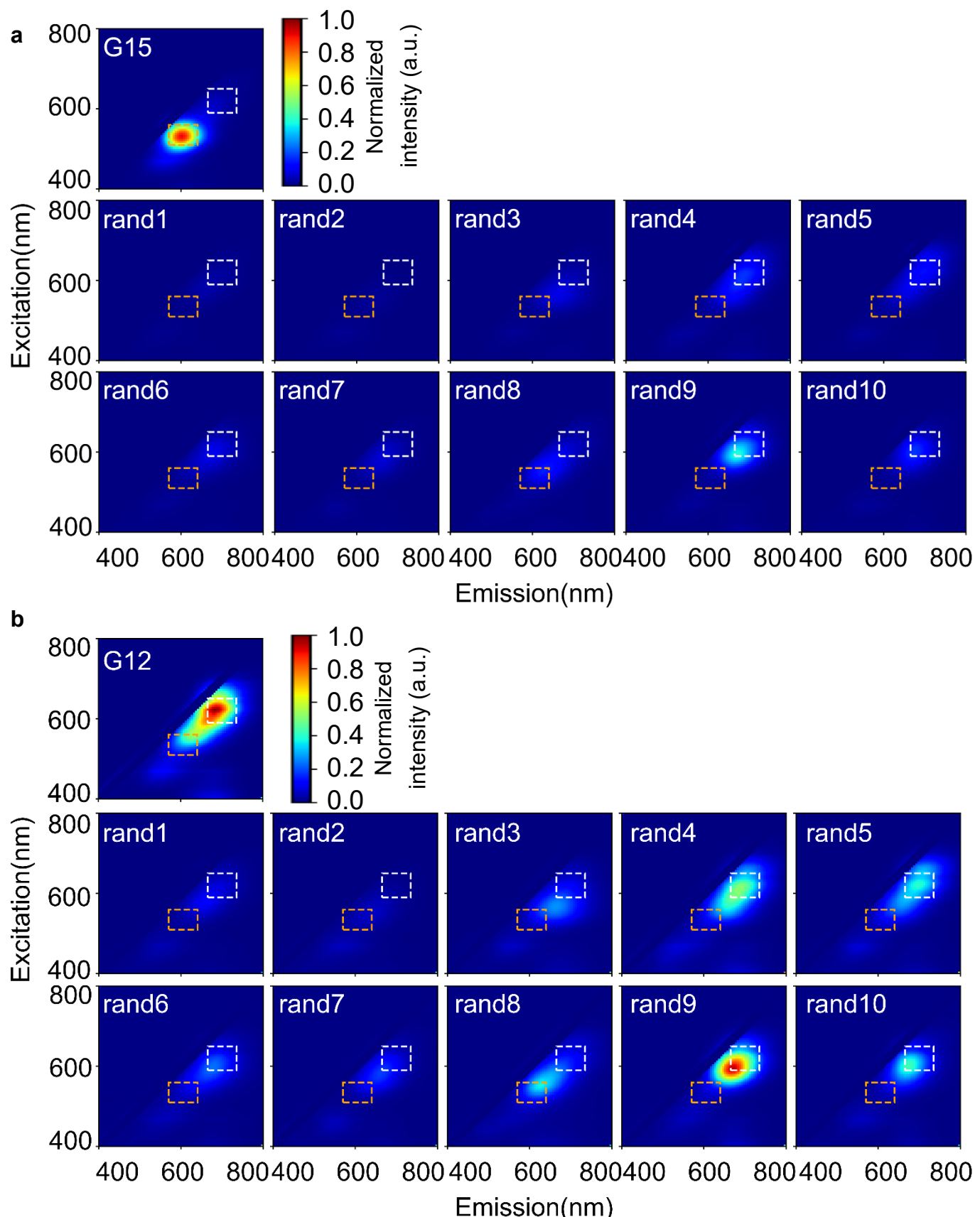


Figure S28 | 2D spectra of randomly designed NCBs. Ten activators are randomly designed and evaluated in test tubes. The enhancement ratio of rand8 passed the threshold in the yellow channel, while rand4, rand5, rand9 and rand10 passed the threshold in the red channel (**Table S8**). Fluorescence intensity normalized to G15 peak intensity (**a**) and G12 peak intensity (**b**). The white dashed box represents the integrated region of red channel (Ex/Em: 620/60, 700/75 nm), and the orange dashed box represents the integrated region of yellow channel (Ex/Em: 535/50, 605/70 nm).

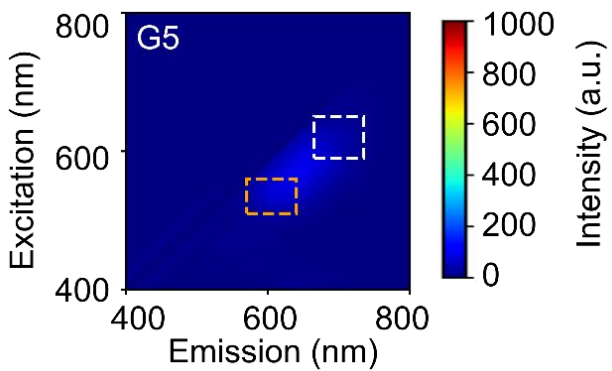


Figure S29 | 2D spectra of G5 NCBs. Based on the design rules discussed in **Fig. 2**, we speculated that this G5 activator (CCCCCCGCGGGGTTTCCC) would lead to a bright NCB. However, the result was actually a low red enhancement ratio (39, as compared to 439 for G12). This result clearly indicated that segments do not work alone – cooperativities among the segments determine the activation color and intensity of an NCB.

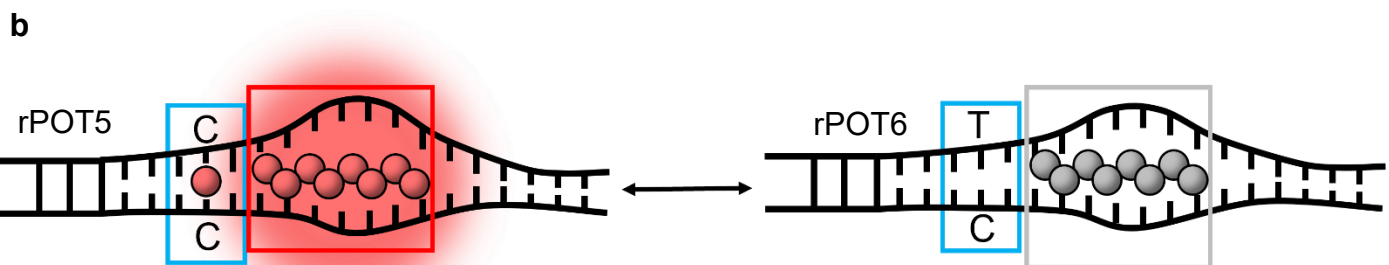
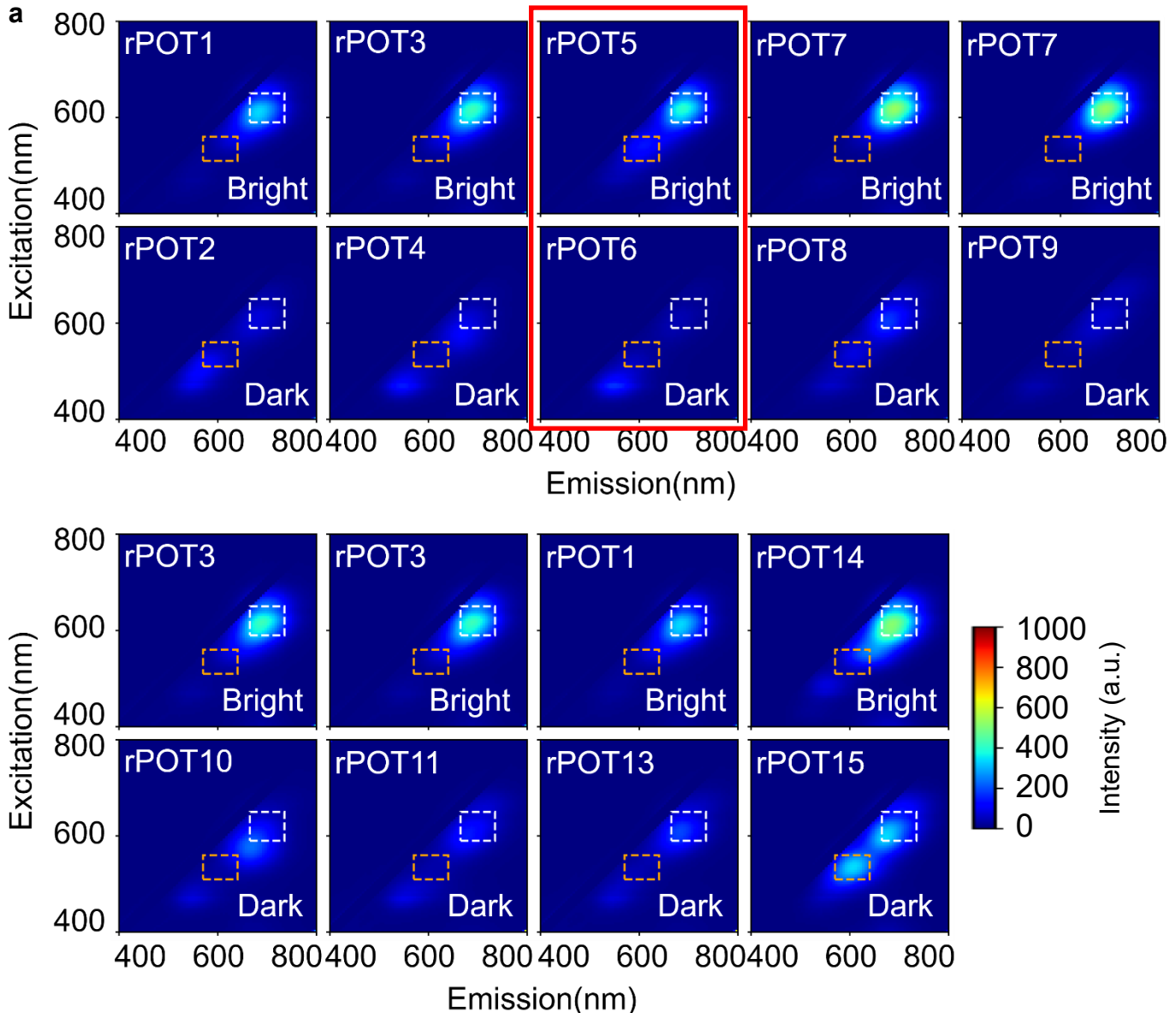


Figure S30 | 2D spectra of red POT candidates. **a** Based on chip selection results, 9 sets of red POT candidates are evaluated in test tubes. All these candidates have their POT difference ratios greater than 1.7, with the largest difference ratio of 9.12 (rPOT5/rPOT6 NCBs, highlighted in solid red box, **Table S8**). **b** Based on the hotspots from **Fig. 3**, we hypothesized that the disruption of silver-mediated pair C-Ag⁺-C would darken red NCB samples and form red POT pairs. The white dashed box represents the integrated region of red channel (Ex/Em: 620/60, 700/75 nm), and the orange dashed box represents the integrated region of yellow channel (Ex/Em: 535/50, 605/70 nm). The blue box represents the hotspots of red POTs. The red and gray boxes represent the bag position of bright member of red POTs and its counterpart, respectively.

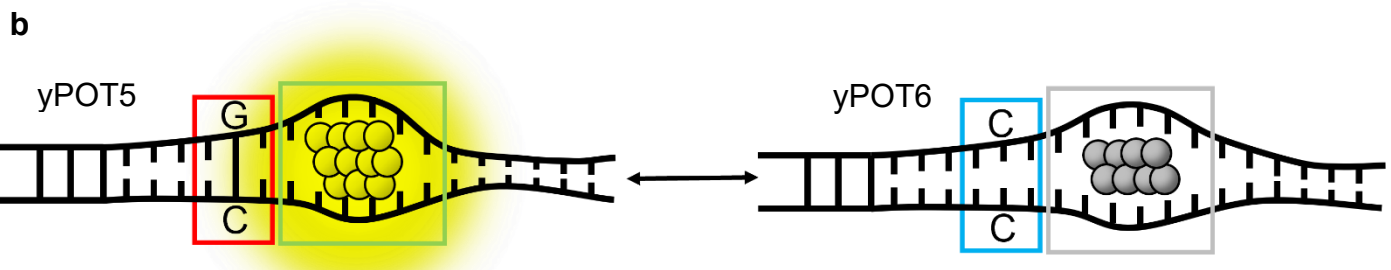
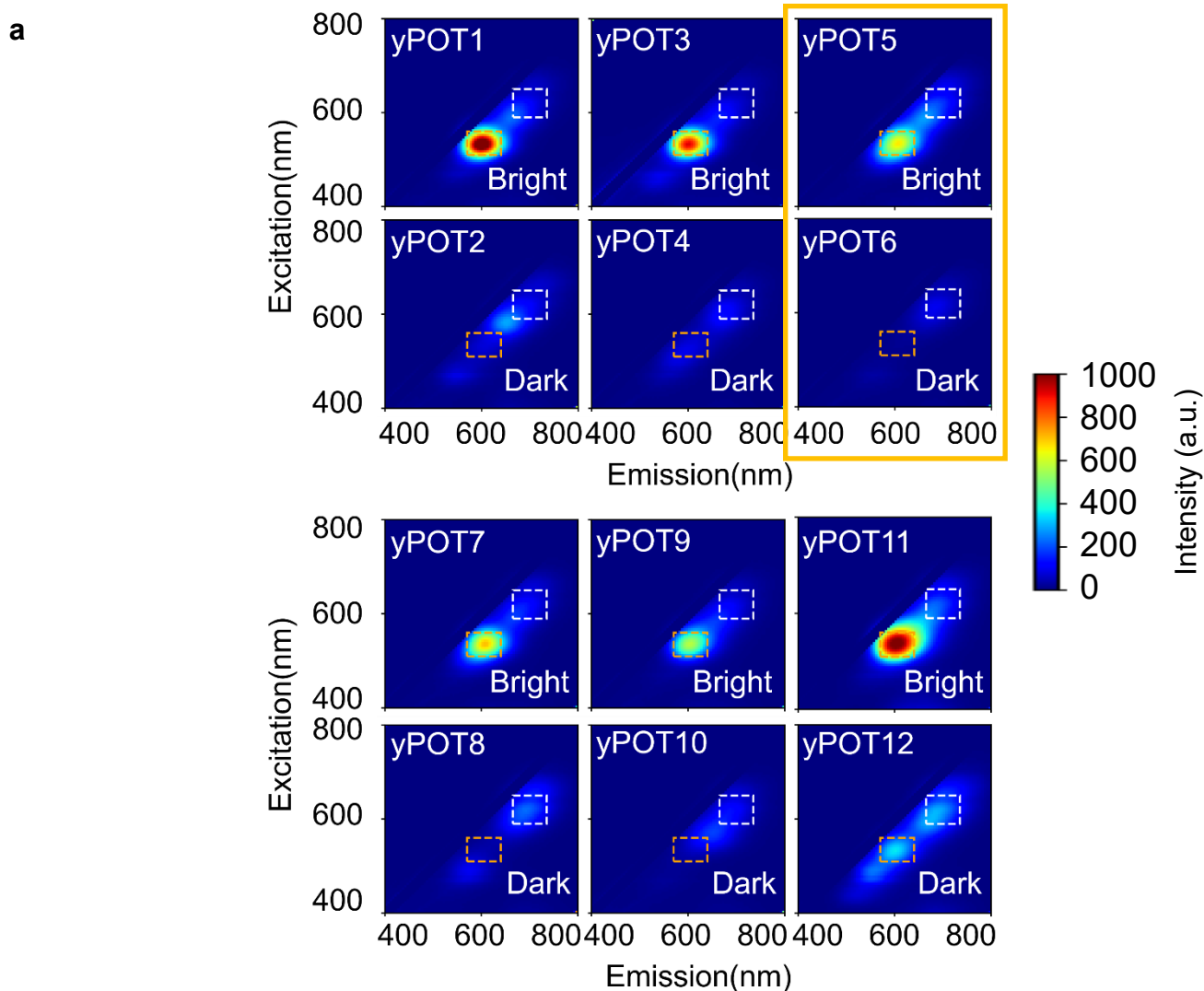


Figure S31 | 2D spectra of yellow POT candidates. **a** Based on chip selection results, 9 sets of yellow POT candidates are evaluated in test tubes. All these candidates have their POT difference ratios greater than 3.0, with the largest difference ratio of 37.04 (yPOT5/yPOT6 NCBs, highlighted in solid orange box, **Table S9**). **b** Based on the hotspots from **Fig. 3**, we hypothesized that the disruption of WC pair, GC pairing, would darken yellow NCB samples and form yellow POT pairs. The white dashed box represents the integrated region of red channel (Ex/Em: 620/60, 700/75 nm), and the orange dashed box represents the integrated region of yellow channel (Ex/Em: 535/50, 605/70 nm). The blue box represents the hotspots of yellow POTs. The gold and gray boxes represent the bag position of bright member of yellow POTs and its counterpart, respectively.

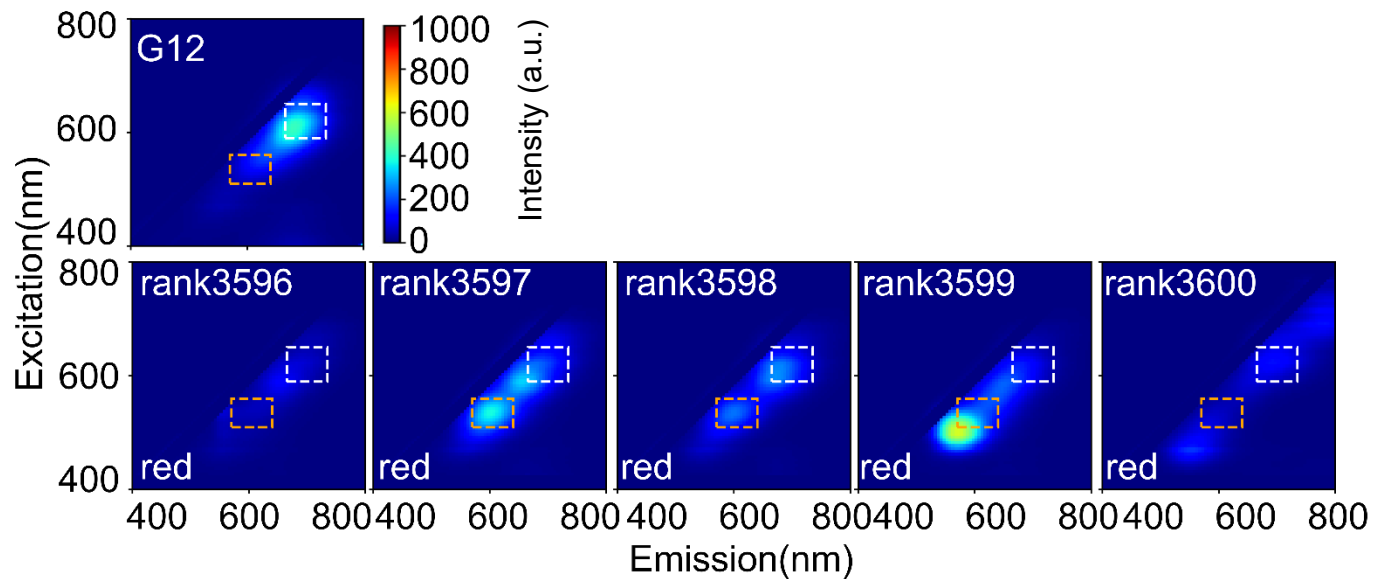


Figure S32 | 2D spectra of red NCBs near ranking 3,600. As we apply top 3,600 sequences as our bright class to perform ML modeling. We evaluate the fluorescence intensity of the NCBs ranking near 3,600. The median enhancement ratio 145 was set as our threshold to evaluate the rationally designed red NCBs.

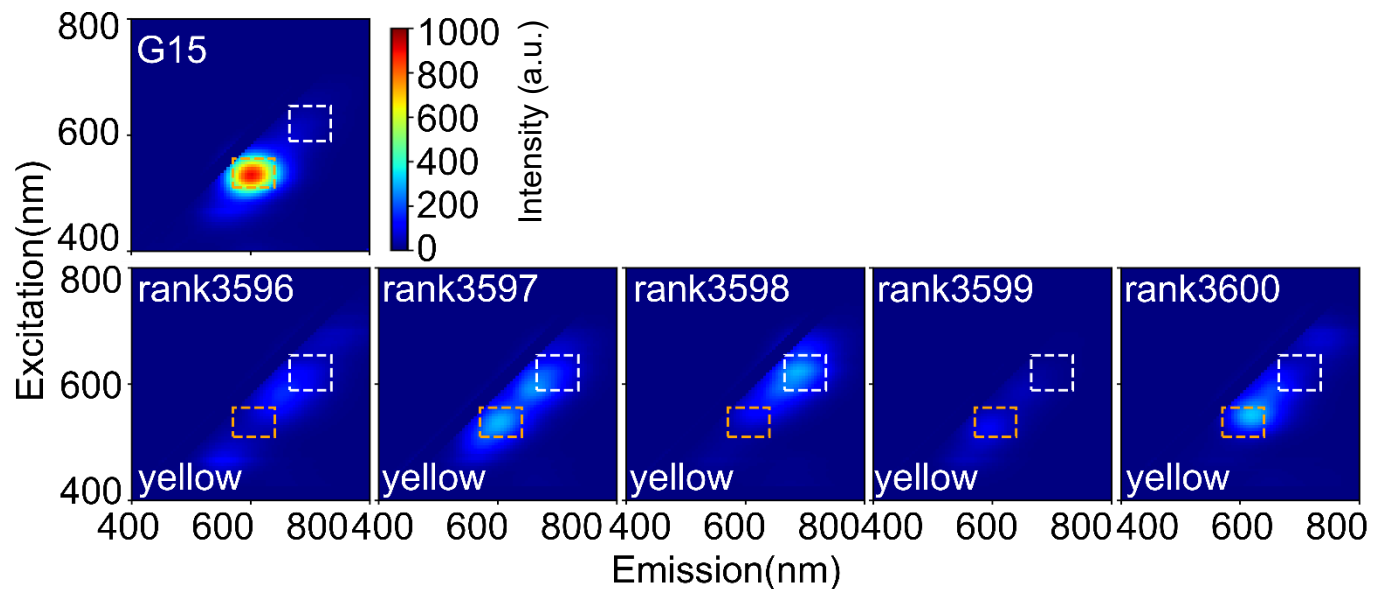


Figure S33 | 2D spectra of yellow NCBs near ranking 3,600. As we apply top 3,600 sequences as our bright class to perform ML modeling. We evaluate the fluorescence intensity of the NCBs ranking near 3,600. The median enhancement ratio 66 was set as our threshold to evaluate the rationally designed yellow NCBs.

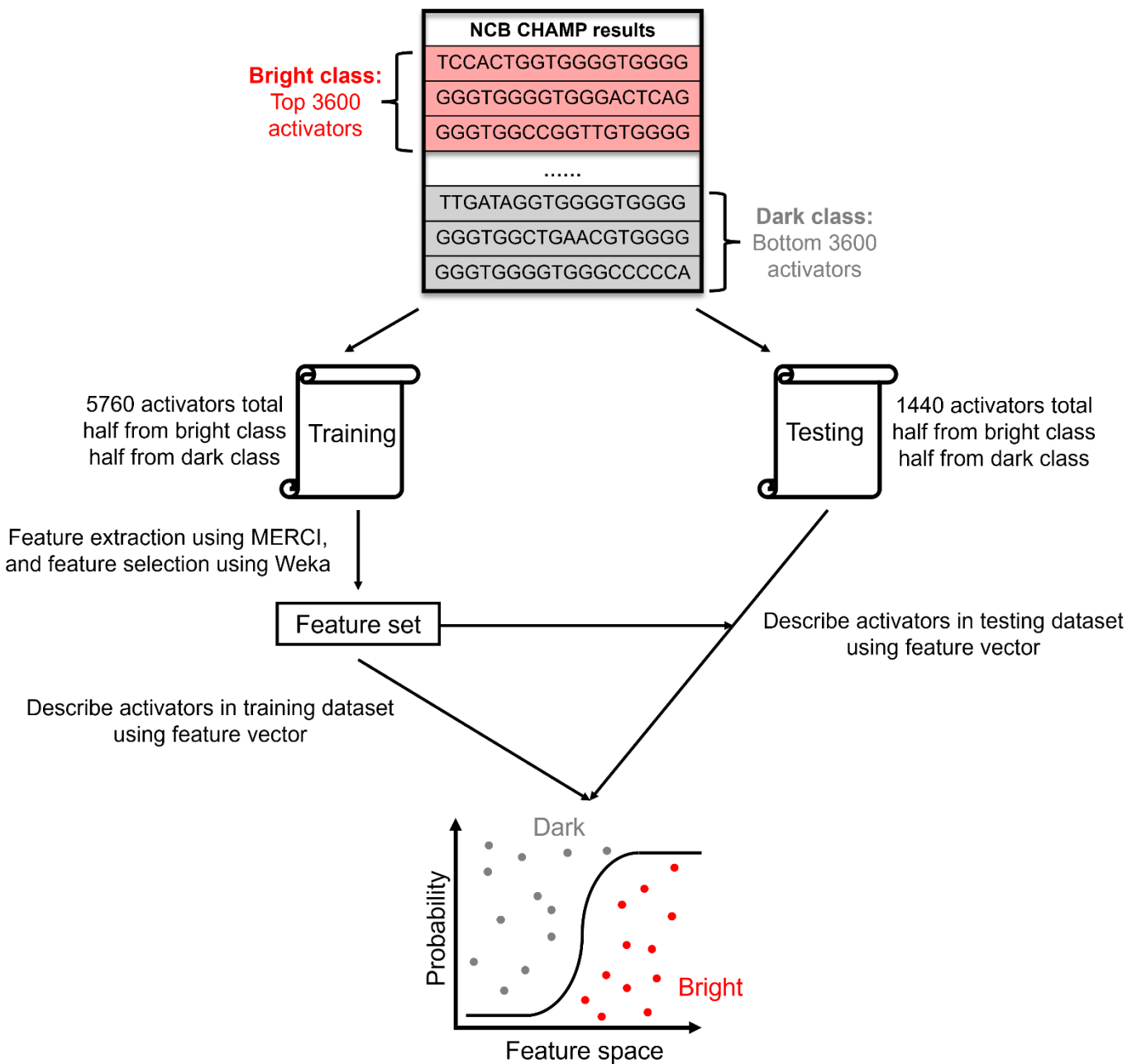


Figure S34 | Workflow for establishing machine learning models to classify screened NCBs or NCB candidates. In this report, we performed 5-fold CV to classify our library sequences. Following the approaches proposed by Copp and Gwinn¹¹⁻¹³, we labeled the top 30% NCBs as “bright” class and the bottom 30% as “dark” class. The feature extraction process was proceeded using MERCI¹⁴. The extracted motifs were processed with Python scripts to include the position information. We then identified the most discriminative set of features using Weka.¹⁵ Based on the selected features, a number of models were established for classifying the chip screening results and we found the model built on LR has the best performance.

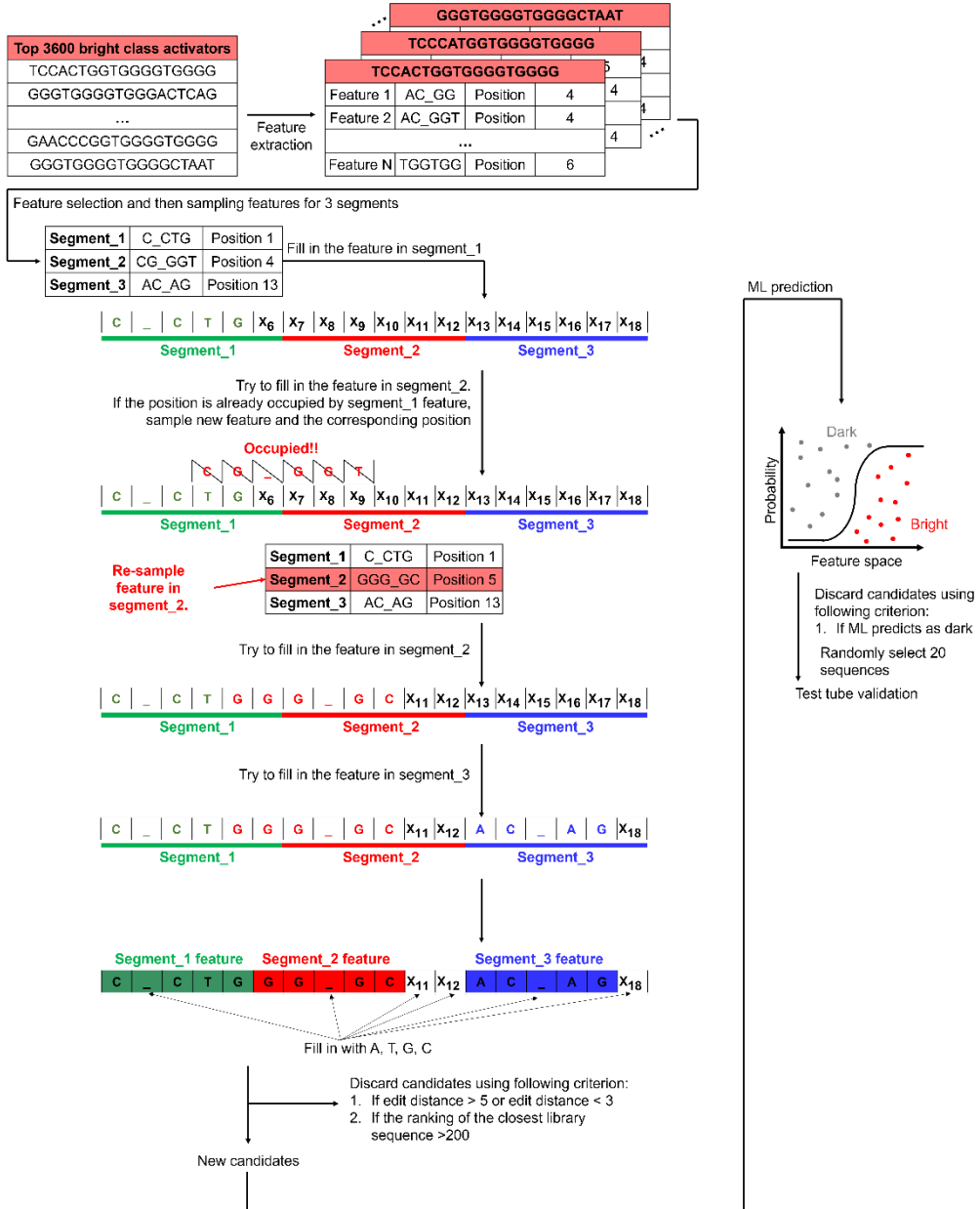


Figure S35 | Workflow to rationally design bright NCBs. Based on the most discriminative features identified by Weka, we sampled the distribution of these features in each segment and generated a list of common motifs with their corresponding positions. To construct a red NCB candidate, we assigned 3 features to the blank 18-nt template, starting with feature_1 insertion into segment_1. As feature_2 might have an overlap with feature_1 when being inserted into segment_2. In that situation, the design algorithm would replace feature_2 with another feature to ensure no overlap. However, if any two features shared identical bases at their overlapping site, they were considered as “compatible” and could be inserted into the same template. For example, as shown above, feature C_CTG (positions 1-5) and feature GGG_GC (positions 5-10) shared a guanine base at the overlapping site (position 5). Consequently, they were compatible and were used in constructing a bright NCB candidate. The same procedure was repeated until a compatible feature for segment_3 was found. Once all three features were inserted into the template, the remaining blank positions were filled up based on the composition popularity (at the same positions) from the bright class sequences. The edit distance^{13,16} of the new candidate was then assessed. We only selected new candidates with edit distance between 3 to 5 from the top 200 bright activators screened on chip for test-tube investigation (**Table S6-S7**).

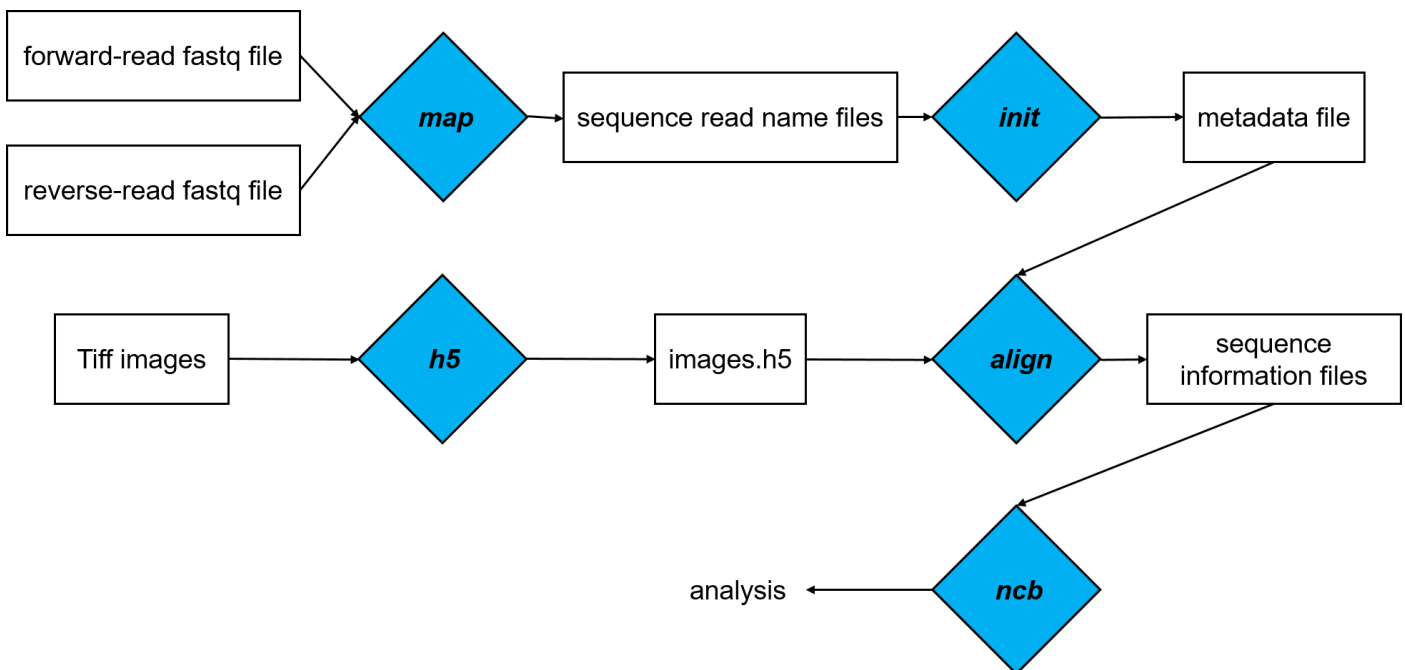


Figure S36 | CHAMP workflow. A custom bioinformatics and imaging processing pipeline named CHAMP (Chip-Hybridized Associated Mapping Platform) was developed by Finkelstein's group and the detailed algorithm description can be found in ref. 6. CHAMP helped decipher the activator sequence behind each activated NCB spot (termed the NCB-CHAMP selection method, **Fig. 1c** and **Supplementary Fig. S4-S5**). In brief, mapping the alignment markers was done at four stages. First, a rough alignment was carried out using Fourier-based cross correlation, followed by a precision alignment using least-squares constellation mapping between FASTQ and *de novo* extracted NCB spots. We built up the consensus sequences and their corresponding information (e.g., lane number, tile number, and x-y coordinates) at all reported positions in the FASTQ file using the **map** command. Second, the **init** command was executed to record the metadata of imaging settings (e.g., rotation and scaling). Third, the **h5** command was applied to generate a single hdf5 file containing all 512×512 PhiX fiducial marker images. Fourth, the **align** command transformed the processed sequence information into pseudo-images and performed precise alignment. The output files were saved individually by image positions. The content included x, y coordinates of each sequence and the corresponding sequence ID. To analyze our NCB images, we developed an additional function named **ncb**, which corrected the uneven illumination using flat-field correction. A bootstrap method was then performed to derive the median intensity of each activator in order to rank the NCB brightness (**Supplementary Fig. S36**).

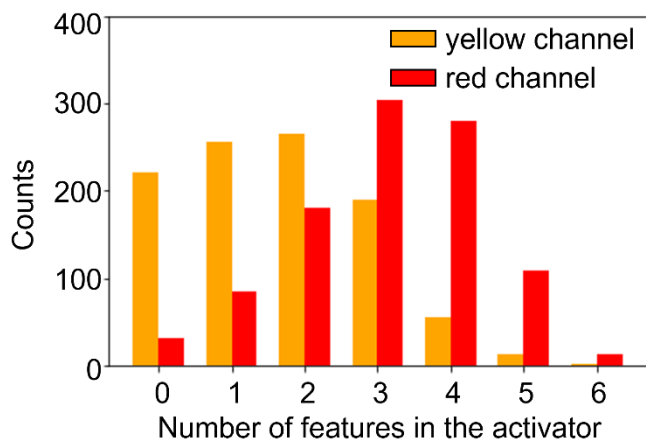


Figure S37 | Feature distribution for the top 1,000 library sequences for red and yellow channels. By evaluating the selected bright features within the top 1,000 library sequences for red and yellow channels, we found the optimal number of features to create bright NCBs would be 2 and 3 for yellow and red channels, respectively.

Table S1: Sequences of probes and library designs used in this report.

a. RE strand is used for restriction enzyme digestion (MauBI). The three Atto probes are used for digestion evaluation and NCB-CHAMP alignment. **b.** The 6-segment and 9-segment interrogation of library_1. **c.** Three different library designs. For each of our library sequences on *MiSeq* chip, it consists of six parts: P5 (light blue), SP1 (gold), library sequence (gray for hybridization segment, purple for activator, and dark blue for restriction site), SP2 (orange), barcode (red), and P7 (green). P5 and P7 are adapters for surface attachment. SP1 and SP2 are sequencing-by-synthesis primer binding sites. Barcodes are reserved and used by *Illumina*. The 30-nt-long hybridization segment is for C55 hybridization and the 18-nt-long activator part is where we call “the library”. As for the library size, library_1 contains 12,286 sequences, library_2 contains 12,286 sequences, and library_3 contains 16,255 sequences. The ‘**CG**’ represents the remaining nucleotides after cleavage by a restriction enzyme, and the vertical line represents the cutting site.

a

Acronym	Sequence (5' → 3')
C55	CCC CCT TAA TCC CCC TAT AAT AAA TTT TAA ATA TTA TTT ATT AAT
G15	ATT AAT AAA TAA TAT TTA AAA TTT ATT ATA GGG TGG GGT GGG GTG GGG
G12	ATT AAT AAA TAA TAT TTA AAA TTT ATT ATA ATC CGG GGT GGG GTG GGG
RE strand	CAG ACG TGT GCT CTT CCG ATC TCG CGC GCG NN
Atto647N-tagged comp_MauBI	/5ATTO647N/ CAG ACG TGT GCT CTT CCG ATC TCG CGC GCG NN
Atto647N-tagged AT	/5ATTO647N/ CCC CCT TAA TCC CCC TAT AAT AAA TTT TAA ATA TTA TTT ATT AAT
Atto488_cPhiX	/5Alex488N/CG GTC TCG GCA TTC CTG CTG AAC CGC TCT TCC GAT C
Forward primer	AAT GAT ACG GCG ACC ACC GAG A
Reverse primer	CAA GCA GAA GAC GGC ATA CGA GA
G15 (90 nt)	ATT AAT AAA TAA TAT TTA AAA TTT ATT ATA GGG TGG GGT GGG GTG GGG AGA TCG GAA GAG CAC ACG TCT GAA CTC CAG TCA CTT GTT CAT

b 6-segment interrogation and 9-segment interrogation in library_1

Acronym	Sequence (5' → 3')
The 6-segment interrogation	
Segment_11	ATT AAT AAA TAA TAT TTA AAA TTT ATT ATA <u>NNN</u> TGG GGT GGG GTG GGG
Segment_12	ATT AAT AAA TAA TAT TTA AAA TTT ATT ATA GGG <u>NNN</u> GGT GGG GTG GGG
Segment_21	ATT AAT AAA TAA TAT TTA AAA TTT ATT ATA GGG TGG <u>NNN</u> GGG GTG GGG
Segment_22	ATT AAT AAA TAA TAT TTA AAA TTT ATT ATA GGG TGG GGT <u>NNN</u> GTG GGG
Segment_31	ATT AAT AAA TAA TAT TTA AAA TTT ATT ATA GGG TGG GGT GGG <u>NNN</u> GGG
Segment_32	ATT AAT AAA TAA TAT TTA AAA TTT ATT ATA GGG TGG GGT GGG GTG <u>NNN</u>

The 9-segment interrogation	
Segment_11	ATT AAT AAA TAA TAT TTA AAA TTT ATT ATA NNG TGG GGT GGG GTG GGG
Segment_12	ATT AAT AAA TAA TAT TTA AAA TTT ATT ATA GN G NGG GGT GGG GTG GGG
Segment_13	ATT AAT AAA TAA TAT TTA AAA TTT ATT ATA GGG TNN GGT GGG GTG GGG
Segment_21	ATT AAT AAA TAA TAT TTA AAA TTT ATT ATA GGG TGG NNT GGG GTG GGG
Segment_22	ATT AAT AAA TAA TAT TTA AAA TTT ATT ATA GGG TGG GN G NGG GTG GGG
Segment_23	ATT AAT AAA TAA TAT TTA AAA TTT ATT ATA GGG TGG GGT GNN GTG GGG
Segment_31	ATT AAT AAA TAA TAT TTA AAA TTT ATT ATA GGG TGG GGT GGG NNG GGG
Segment_32	ATT AAT AAA TAA TAT TTA AAA TTT ATT ATA GGG TGG GGT GGG GTN NGG
Segment_11	ATT AAT AAA TAA TAT TTA AAA TTT ATT ATA GGG TGG GGT GGG GTG GNN

c sequence information of library_1, library_2 and library_3

Acronym	Sequence (5' → 3')
Canonical activator G15 in library_1	AATGATA <u>CGGCGACCACCGAGA</u> (P5) TCTACACT <u>CTTCCCTACACGACGCTTCCGATCT</u> (SP1) ATTAATAATAATTTAAAATTATTATA <u>GGGTGGGGTGGGGTGGGG</u> (activator) <u>CG CGCGCG</u> (restriction site) AGATCGGAAGAGCACACGTCTGA <u>ACTCCAGTCAC</u> (SP2) GTAGAG (barcode) ATCTCGTATGCCGT <u>CTTGCTTG</u> (P7)
Canonical activator G15 in library_2 and library_3	AATGATA <u>CGGCGACCACCGAGA</u> (P5) TCTACACT <u>CTTCCCTACACGACGCTTCCGATCT</u> (SP1) ATTAATAATAATTTAAAATTATTATA <u>GGGTGGGGTGGGGTGGGG</u> (activator) AGATCGGAAGAGCACACGTCTGA <u>ACTCCAGTCAC</u> (SP2) GTAGAG (barcode) ATCTCGTATGCCGT <u>CTTGCTTG</u> (P7)
Segment_1 activators In library_1	AATGATA <u>CGGCGACCACCGAGA</u> (P5) TCTACACT <u>CTTCCCTACACGACGCTTCCGATCT</u> (SP1) ATTAATAATAATTTAAAATTATTATA <u>NNNNNNNGGTGGGGTGGGG</u> (activator) <u>CG CGCGCG</u> (restriction site) AGATCGGAAGAGCACACGTCTGA <u>ACTCCAGTCAC</u> (SP2) TTGTTC (barcode) ATCTCGTATGCCGT <u>CTTGCTTG</u> (P7)
Segment_2 activators in library_1	AATGATA <u>CGGCGACCACCGAGA</u> (P5) TCTACACT <u>CTTCCCTACACGACGCTTCCGATCT</u> (SP1) ATTAATAATAATTTAAAATTATTATA <u>GGGTGGNNNNNGTGGGG</u> (activator) <u>CG CGCGCG</u> (restriction site) AGATCGGAAGAGCACACGTCTGA <u>ACTCCAGTCAC</u> (SP2) TTGTTC (barcode) ATCTCGTATGCCGT <u>CTTGCTTG</u> (P7)
Segment_3 activators In library_1	AATGATA <u>CGGCGACCACCGAGA</u> (P5) TCTACACT <u>CTTCCCTACACGACGCTTCCGATCT</u> (SP1) ATTAATAATAATTTAAAATTATTATA <u>GGGTGGGGTGGGNNNNN</u> (activator) <u>CG CGCGCG</u> (restriction site) AGATCGGAAGAGCACACGTCTGA <u>ACTCCAGTCAC</u> (SP2) TTGTTC (barcode) ATCTCGTATGCCGT <u>CTTGCTTG</u> (P7)

Segment_1 activators In library_2	AATGATA <u>CGGCACCACCGAGA</u> (P5) TCTACACT <u>CTTCCCTACACGACGCTTCCGATCT</u> (SP1) ATTAATAAAATAATTTAAAATTATTATA <u>GGGN>NNNNNGGGTGGGG</u> (activator) AGATCGGAAGAGCACACGTCTGA <u>ACTCCAGTCAC</u> (SP2) TTGTTTC (barcode) ATCTCGTATGCCGTCTGCTTG (P7)
Segment_2 activators In library_2	AATGATA <u>CGGCACCACCGAGA</u> (P5) TCTACACT <u>CTTCCCTACACGACGCTTCCGATCT</u> (SP1) ATTAATAAAATAATTTAAAATTATTATA <u>GGGTGGGGTN>NNNNNGGG</u> (activator) AGATCGGAAGAGCACACGTCTGA <u>ACTCCAGTCAC</u> (SP2) TTGTTTC (barcode) ATCTCGTATGCCGTCTGCTTG (P7)
Segment_3 activators In library_2	AATGATA <u>CGGCACCACCGAGA</u> (P5) TCTACACT <u>CTTCCCTACACGACGCTTCCGATCT</u> (SP1) ATTAATAAAATAATTTAAAATTATTATA <u>NNNTGGGGTGGGTGNNN</u> (activator) AGATCGGAAGAGCACACGTCTGA <u>ACTCCAGTCAC</u> (SP2) TTGTTC (barcode) ATCTCGTATGCCGTCTGCTTG (P7)
Segment_1 activators In library_3	AATGATA <u>CGGCACCACCGAGA</u> (P5) TCTACACT <u>CTTCCCTACACGACGCTTCCGATCT</u> (SP1) ATTAATAAAATAATTTAAAATTATTATA <u>NNNTGGNNNGGGTGGGG</u> (activator) AGATCGGAAGAGCACACGTCTGA <u>ACTCCAGTCAC</u> (SP2) TTGTTC (barcode) ATCTCGTATGCCGTCTGCTTG (P7)
Segment_2 activators in library_3	AATGATA <u>CGGCACCACCGAGA</u> (P5) TCTACACT <u>CTTCCCTACACGACGCTTCCGATCT</u> (SP1) ATTAATAAAATAATTTAAAATTATTATA <u>GGGN>NNNNNGGTNNNGTGGGG</u> (activator) AGATCGGAAGAGCACACGTCTGA <u>ACTCCAGTCAC</u> (SP2) TTGTTC (barcode) ATCTCGTATGCCGTCTGCTTG (P7)
Segment_3 activators library_3	AATGATA <u>CGGCACCACCGAGA</u> (P5) TCTACACT <u>CTTCCCTACACGACGCTTCCGATCT</u> (SP1) ATTAATAAAATAATTTAAAATTATTATA <u>GGGTGGNNNGGGNNNGGG</u> (activator) AGATCGGAAGAGCACACGTCTGA <u>ACTCCAGTCAC</u> (SP2) TTGTTC (barcode) ATCTCGTATGCCGTCTGCTTG (P7)
Segment_4 activators In library_3	AATGATA <u>CGGCACCACCGAGA</u> (P5) TCTACACT <u>CTTCCCTACACGACGCTTCCGATCT</u> (SP1) ATTAATAAAATAATTTAAAATTATTATA <u>GGGTGGGGTN>NNNGTGNNN</u> (activator) AGATCGGAAGAGCACACGTCTGA <u>ACTCCAGTCAC</u> (SP2) TTGTTC (barcode) ATCTCGTATGCCGTCTGCTTG (P7)

Table S2: Test-tube investigation of selected bright red and dark activator candidates.

To validate our NCB-CHAMP selection method, twenty top-ranked and twenty bottom-ranked activators are further investigated in test tubes. **a.** Using G12 NCB (ATCCGGGGTGGGGTGGGG) as the standard for red emitter comparison, 17 out 20 bright red candidates are found brighter than G12 NCB in test tubes (also see **Fig. S13**). **b.** 17 out 20 dark candidates are found darker than G12 NCB in test tubes (**Fig. S14**). The formulas to compute “enhancement ratio” and “improvement ratio” are described in **Methods**. In short, we first calculate the volumetric integrated intensity (**Fig. S2**) from the 2D spectrum of the sample in the red channel (Ex: 620/60 nm, Em: 700/75 nm). From there we calculate the enhancement ratio:

$$\text{Enhancement ratio} = (I_{\text{NCB}} - I_{\text{NC probe}}) / (I_{\text{NC probe}} - I_{\text{background}})$$

where I_{NCB} stands for the volumetric integrated intensity of NCB in red of yellow window, $I_{\text{NC probe}}$ represents the volumetric integrated intensity of dark AgNC on C55 probe, and $I_{\text{background}}$ is the volumetric integrated intensity of buffer (i.e., sodium phosphate buffer). The improvement ratio is simply the ratio of the enhancement ratio of an NCB to that of the standard red NCB (G12). False selections are highlighted in gray below.

a Selected red bright NCB candidates:

ID	Activator (5' → 3')	Enhancement ratio in red channel	Improvement ratio (compared to G12)
G12	ATCCGGGGTGGGGTGGGG	439	1
rAct1	TCCATTGGTGGGGTGGGG	1292	2.94
rAct2	TCCAATGGTGGGGTGGGG	1247	2.84
rAct3	TCCATAGGTGGGGTGGGG	1229	2.80
rAct4	ATCCGTGGTGGGGTGGGG	601	1.37
rAct5	TCCTATGGTGGGGTGGGG	756	1.72
rAct6	TCTCATGGTGGGGTGGGG	498	1.13
rAct7	ATCCCAGGTGGGGTGGGG	973	2.22
rAct8	CCTTCTGGTGGGGTGGGG	532	1.21
rAct9	CACATTGGTGGGGTGGGG	764	1.74
rAct10	CCCCAAGGTGGGGTGGGG	669	1.52
rAct11	CCTTGAGGTGGGGTGGGG	575	1.31
rAct12	TCACTAGGTGGGGTGGGG	616	1.40
rAct13	ACTCGTGGTGGGGTGGGG	583	1.33
rAct14	CCTGCAGGTGGGGTGGGG	678	1.54
rAct15	GGGTGGGGTGGGGCTAGA	833	1.90
rAct16	TGGGACGGTGGGGTGGGG	694	1.58
rAct17	TGAACAGGTGGGGTGGGG	516	1.18
rAct18	GCTACAGGTGGGGTGGGG	269	0.61
rAct19	CGGTTTGGTGGGGTGGGG	166	0.38
rAct20	CGCTTCGGTGGGGTGGGG	201	0.46

b Selected dark candidates:

ID	Activator (5' → 3')	Enhancement ratio in red channel	improvement ratio (compared to G12)
G12	ATCCGGGGTGGGGTGGGG	439	1
rAct21	GGGTGGGGTGGGACGCTA	221	0.51
rAct22	ATCTGAGGTGGGGTGGGG	236	0.54
rAct23	GGGTGGGGTGGGGACATT	256	0.58
rAct24	AAGTTTGGTGGGGTGGGG	139	0.32
rAct25	AACGATGGTGGGGTGGGG	404	0.92
rAct26	TGGCTTGGTGGGGTGGGG	272	0.62
rAct27	CTGCTTGGTGGGGTGGGG	423	0.96
rAct28	GGGTGGGGTGGGGAGATC	587	1.34
rAct29	CTGCCCGGTGGGGTGGGG	347	0.79
rAct30	AAAAGGGGTGGGGTGGGG	192	0.44
rAct31	ACGTTTGGTGGGGTGGGG	575	1.30
rAct32	GGTGCAGGTGGGGTGGGG	124	0.28
rAct33	ACAATAGGTGGGGTGGGG	375	0.86
rAct34	GGGTGGGGTGTGGTGGGG	243	0.55
rAct35	GGGTGGCGATTAGTGTGGGG	148	0.35
rAct36	GGGTGGTAATGTGTGGGG	78	0.19
rAct37	GGGTGGGGTGGGTGTAGG	310	0.71
rAct38	GGGTGGGTTATGTGGGG	44	0.10
rAct39	GGGTGGTCAAAAGTGGGG	81	0.19
rAct40	GGGTGGCCTCCAGTGGGG	571	1.29

Table S3: Test-tube investigation of selected bright yellow activator candidates.

To validate our NCB-CHAMP selection method, ten top-ranked yellow activators are further investigated in test tubes. **A.** Using G15 NCB (GGGTGGGTGGGTGGGG) as the standard for yellow emitter comparison, all 10 bright yellow candidates are found brighter than G15 NCB in test tubes (also see **Fig. S15**). The formulas to compute “enhancement ratio” and “improvement ratio” are described in **Methods**. In short, we first calculate the volumetric integrated intensity (**Fig. S2**) from the 2D spectrum of the sample in the yellow channel (Ex: 535/50 nm, Em: 605/70 nm). From there we calculate the enhancement ratio:

$$\text{Enhancement ratio} = (I_{\text{NCB}} - I_{\text{NC probe}}) / (I_{\text{NC probe}} - I_{\text{background}})$$

where I_{NCB} stands for the volumetric integrated intensity of NCB in yellow window, $I_{\text{NC probe}}$ represents the volumetric integrated intensity of dark AgNC on C55 probe, and $I_{\text{background}}$ is the volumetric integrated intensity of buffer (i.e., sodium phosphate buffer). The improvement ratio is simply the ratio of the enhancement ratio of an NCB to that of the standard yellow activator (G15).

ID	Sequence (5' → 3')	Enhancement ratio	Improvement ratio (compared to G15)
G15	GGGTGGGTGGGTGGGG	553	1
yAct1	CAGGTGGGTGGGTGGGG	988	1.79
yAct2	TTTGTGGGTGGGTGGGG	872	1.58
yAct3	TGTGTGGGTGGGTGGGG	951	1.72
yAct4	TTGGTGGGTGGGTGGGG	1125	2.03
yAct5	AAGTTGGGTGGGTGGGG	924	1.67
yAct6	AGTTGAGGTGGGTGGGG	1105	2.00
yAct7	TTGTGAGGTGGGTGGGG	1009	1.82
yAct8	GTTTGAGGTGGGTGGGG	1045	1.89
yAct9	AGTTTGGGTGGGTGGGG	840	1.52
yAct10	ATGTTGGGTGGGTGGGG	922	1.67

Table S4: Test-tube investigation of 10-guanine activators

Based on chip selection results, ten 10G activators can potentially be brighter than G12 NCB (**Fig. S15**). Test-tube investigation proves that 7 of the selected 10G activators have their enhancement ratios comparable to that of G12 in the red channel (improvement ratio ≥ 0.9). This result indicates that it is possible to create bright red NCBs with fewer numbers of guanine. False selections are highlighted in gray below.

ID	Sequence (5' → 3')	Enhancement ratio	Improvement ratio (compared to G12)
G12	ATCCGGGGTGGGTGGGG	439	1
10G_1	AACCTTGGTGGGTGGGG	415	0.95
10G_2	TCCAATGGTGGGTGGGG	409	0.93
10G_3	ATCCATGGTGGGTGGGG	397	0.91
10G_4	ATCCCAGGTGGGTGGGG	413	0.95
10G_5	TACCATGGTGGGTGGGG	527	1.21
10G_6	GGGTGGTCCCCCGTGGGG	240	0.54
10G_7	AACCATGGTGGGTGGGG	480	1.09
10G_8	CTCCATGGTGGGTGGGG	473	1.09
10G_9	ACATCAGGTGGGTGGGG	204	0.47
10G_10	GGGTGGCCCCCGTGGGG	221	0.51

Table S5: Test-tube investigation for activators having at least 12 guanines

Based on chip selection results, ten 12G activators can potentially be darker than G12 NCB (**Fig. S15**). Test-tube investigation proves that all of the selected 12G activators are darker than G12 in the red channel (improvement ratio < 0.6).

ID	Sequence (5' → 3')	Enhancement ratio	Improvement ratio (compared to G12)
G12	ATCCGGGGTGGGGTGGGG	439	1
12G_1	GGGTGGTCGGACGTGGGG	61	0.15
12G_2	GGGTGGTGTCAAGGTGGGG	124	0.29
12G_3	GGGTGGAAGAGGGTGGGG	51	0.12
12G_4	GGGTGGTTGCTGGTGGGG	260	0.59
12G_5	GGGTGGGTCGCCGTGGGG	126	0.29
12G_6	GGGTGGAGTGATGTGGGG	45	0.11
12G_7	GGGTGGTGAGACGTGGGG	26	0.06
12G_8	GGGTGGGCTGACGTGGGG	31	0.08
12G_9	GGGTGGAAGAGGTGTGGGG	57	0.14
12G_10	GGGTGGACGACGGTGGGG	17	0.05

Table S6: Test-tube investigation of rationally designed bright red NCBs.

Twenty activators are designed based on the machine learning results and evaluated in test tubes. Following the observation shown in **Supplementary Fig. S37**, the new red candidates were generated if three bright red features were presented in the sequences as shown below. On average, the enhancement ratio was 291 for these twenty and the mean edit distance was 4.0. Here the enhancement ratio of 145 was set as the cutoff for bright yellow NCBs (**Table S9a**). Three out of the 20 rationally designed red NCBs below showed either low emission (rPred19 and rPred20, highlighted in gray) or yellow emission (rPred14, highlighted in yellow). Thus, the overall test-tube validation accuracy was 85%. Among the 20 NCBs below, rPred9 NCB was the brightest (1.30-fold brighter than G12 NCB, highlighted in red).

ID	Activator (5' → 3')	Emission peak (nm)	Minimal edit distance	Enhancement ratio	Improvement ratio compared to G12	Motif #1	Motif #2	Motif #3
rPred1	TCCCATGCGGGGCTCGGG	655	4	220	0.50	CCC	GGG_C	TC_GG
rPred2	CCCGAAGGGGGGATCGCG	640	4	250	0.57	CCC	GGGGA	TC(CG)
rPred3	CCCGAAGGTGGGCTCTG	655	4	487	1.11	CCC	GA_GGT	C_CTG
rPred4	TACCAAGGGGGAACGGG	685	4	167	0.38	CA_GG	GGGGA	AA_GG
rPred5	ACCAGAGGGGTGGGCCCG	645	5	154	0.35	ACC_G	AG_GGT	CCC
rPred6	TCCCAAGGTGGGGGCAG	640	3	198	0.45	CCC	CA_GG	GGGG_C
rPred7	TCCCGAGGTGGGCTGG	685	3	408	0.93	CCC	CG_GGT	CTGG
rPred8	TCCAGCGGGGGAGGGGGC	735	4	184	0.42	TCC_G	GGGGA	GGG_C
rPred9	ATCCCTCGGGGAGGGGGC	670	5	571	1.30	CCC	GGGGA	GGGG_C
rPred10	CATCCGTTGGGGACGGG	685	5	180	0.41	A_CCG	TTGG_G	GGGAC
rPred11	GCCCGAGGGGGGGACGGG	655	3	373	0.85	CCC	C_AGG	GGGAC
rPred12	TCCAGTGGGGGAGCGGG	680	4	505	1.15	TCC_G	GGGGA	GCGG
rPred13	CCCGTAGGGTAGGTTGGG	685	4	316	0.72	CCC	TA_GGT	TT_GG
rPred14	CCCGAAGGGGGGGCATG	580	5	531	1.21	CCC	AA_GG	GGG_C
rPred15	TCCCGCGGGGGGGACGGG	635	3	325	0.74	CCC	GGGA	GGGAC
rPred16	TCCGGACGGGGTGGGG	660	3	277	0.63	TCC_G	AC_GG	TGGGGG
rPred17	TCCCCAGGGGGACTGGGG	640	3	170	0.39	CCC	GGGGA	CTGG
rPred18	ATCCTTCGGGGATCGGG	630	5	380	0.87	CTT_G	GGGGA	A_CGG
rPred19	TCCAAGGGGTGGACTGGC	650	4	101	0.23	AA_GG	AG_GGT	CTGG
rPred20	TACCCAGGGGGACTGGGC	650	4	31	0.07	CCC	CA_GG	ACT_G

Table S7: Test-tube investigation of rationally designed yellow NCBs.

Twenty activators are designed based on the machine learning results and evaluated in test tubes. Following the observation shown in **Supplementary Fig. S37**, the new yellow candidates were generated if two bright yellow features were presented in the sequences as shown below. On average, the enhancement ratio was 532 for these twenty designs and the mean edit distance was 3.5. Here the enhancement ratio of 66 was set as the cutoff for bright yellow NCBs (**Table S9b**). Three out of the 20 rationally designed yellow NCBs below showed either low emission (yPred18, yPred19 and rPred20, highlighted in gray) or red emission (yPred18 and rPred20). Thus, the overall test-tube validation accuracy was 85%. Among the 20 NCBs below, yPred1 NCB was the brightest (2.30-fold brighter than G15 NCB, highlighted in red).

ID	Activator (5' → 3')	Emission peak (nm)	Minimal edit distance	Enhancement ratio	Improvement ratio compared to G15	Motif #1	Motif #2
yPred1	GTGTTGGGTGGTCGGGGG	585	3	1272	2.30	GTG_TG	TGGGTG
yPred2	GGTGTGGGTGGGAAGGGC	595	3	371	0.67	GT_TG	TGGGTG
yPred3	TGTGTGTGGGGATGGGG	595	3	968	1.75	GT_TGG	GGGGG
yPred4	GCTGTGTGGGTGTGGGG	585	3	724	1.31	GT_TGG	GTGTGG
yPred5	GGAGTGGGTGGTGGTGGG	590	3	487	0.88	TGGGTG	GTG_TG
yPred6	TCGGTGTGGTGTGTGGGG	585	4	299	0.54	GTGGTG	GTGTGG
yPred7	TGGTGTGGTTGGCGGGGG	600	3	946	1.71	GT_TGG	T_GCG
yPred8	AGTGTGGTGTGGGGGGG	595	5	619	1.12	GTGGTG	TTG_GG
yPred9	GCTTGGGTGGGTGTGGGC	600	3	448	0.81	GT_TGG	TGGGTG
yPred10	AGTGGGTGTGTGTGGGGG	595	4	680	1.23	GT_TGG	TGGGTG
yPred11	GAGTTAGGGGTGTGGGGC	580	5	885	1.60	GT_AG	GT_TGG
yPred12	AGTGTGGGTGTGTGGGGG	595	3	481	0.87	GT_TGG	TGGGTG
yPred13	GGTGTGGGTGTGTGGGGG	600	3	249	0.45	GT_TGG	TGGGTG
yPred14	GTTGTGGTGGGAGGGGGG	600	4	559	1.01	GTGGTG	GA_GGG
yPred15	GTATGAGTGGGTGTGGGC	600	4	498	0.90	TGGGTG	GTGTGG
yPred16	GTCGTGGTGGTGGTGGGC	600	4	470	0.85	GTGGTG	GTG_TG
yPred17	GAGGTGGTGGTGGTGGGG	595	3	514	0.93	GTGGTG	GTG_TG
yPred18	TGTGGTGAGGGGGAGGGG	665	3	53	0.10	TGA_G	GGGG_A
yPred19	GGTGTGGTGGTGGTGGGC	580	4	65	0.12	GTGGTG	GTG_TG
yPred20	CGTGTGGTTGGGGGGG	685	3	50	0.09	GT_TGG	TTG_GG

Table S8: Test-tube investigation of randomly designed NCBs and G5.

Ten randomly designed activators and a hypothetical bright candidate (G5) designed based on **Fig. 2** conclusion were evaluated in test tubes. Note that we do not preset any threshold of predicted success before selection here. On average, the enhancement ratio of the ten designs in yellow and red channels were 19 and 126, respectively. Since we selected top 30% (3,600) activator sequences as the bright class, we used the median enhancement ratio value from ranking 3,595 to ranking 3,600 sequences as our new criteria for bright/dark categorization, which corresponded to 145 and 66 for red and yellow channels, respectively (see **Table S9**). As a result, 1 out the 10 random sequences was identified as a “bright yellow” activator and 4 out of the 10 random sequences were identified as “bright red” activators.

ID	Sequence (5' → 3')	Emission peak (nm)	Enhancement ratio (yellow)	Improvement ratio (compared to G15)	Enhancement ratio (red)	Improvement ratio (compared to G12)
G5	CCCCCCGCGGGGTTTCCC	645	39	0.09	83	0.19
rand1	AGGGACTAGGTGGCGCT	660	9	0.02	44	0.10
rand2	CGCGTGAGCGAGGTCGAG	630	10	0.02	9	0.02
rand3	GTACGGAGGTGAGCTTGG	660	23	0.04	66	0.15
rand4	TGTGCACAAGAGGGGAGG	685	30	0.05	250	0.57
rand5	GCTGATTGGCGCTTGGG	695	24	0.04	206	0.47
rand6	GGCCGACTTGTGGTAGG	675	24	0.04	92	0.21
rand7	TGAGGGCTGAGACGCCGG	660	19	0.03	53	0.12
rand8	GCTCGGGCCAGGTGGAAG	625	68	0.12	79	0.18
rand9	AGTGGGGATGAGTGTGCA	665	28	0.05	316	0.72
rand10	GCCGGGTTGTAGATGGGT	670	18	0.03	149	0.34

Table S9: Test-tube investigation of red and yellow NCBs ranked near 3600.

As we selected top 30% (3,600) activator sequences as the bright class, we used the median enhancement ratio value from ranking 3,595 to ranking 3,600 sequences as our new criteria for bright/dark categorization, which corresponded to 145 and 66 for red and yellow channels, respectively.

a Red channel

ID	Sequence (5' → 3')	Emission peak (nm)	Enhancement ratio (red)	Improvement ratio (compared to G12)
Rank3596	CTCGAAGGTGGGTGGGG	650	83	0.19
Rank3597	TGGAAAGGTGGGTGGGG	600	239	0.54
Rank3598	CGTAGTGGTGGGTGGGG	670	233	0.53
Rank3599	GAACCCGGTGGGTGGGG	570	143	0.33
Rank3600	GGGTGGGTGGGGTGGGA	550	145	0.33

b Yellow channel

ID	Sequence (5' → 3')	Emission peak (nm)	Enhancement ratio (yellow)	Improvement ratio (compared to G15)
Rank3596	GGGTGGGTGGGTCAATC	655	55	0.10
Rank3597	CGAACGGTGGGTGGGG	600	210	0.38
Rank3598	AAACCGGGTGGGTGGGG	685	66	0.12
Rank3599	GGGTGGATGGCAGTGGGG	590	61	0.11
Rank3600	GGGTGGTGCGAGCGTGGGG	615	182	0.33

Table S10: Test-tube investigation of red POT candidates.

Based on chip selection results, 9 sets of red POT candidates are evaluated in test tubes. All these candidates have their POT difference ratios greater than 1.63, with the largest difference ratio of 8.92 (rPOT5/rPOT6, **Fig. S18**). Single-nucleotide differences in these POTs are marked in red. POT difference ratio is simply the ratio of the enhancement ratios of the twins, which is, POT difference ratio=(Enhancement ratio of bright candidate)/(Enhancement ratio of dark candidate)

ID (Bright)	Sequence (5' → 3')	ID (Dark)	Sequence (5' → 3')	POT difference ratio in red channel (Bright/Dark)
rPOT1	AT <u>C</u> CGTGGTGGGTGGGG	rPOT2	AT <u>I</u> CGTGGTGGGTGGGG	4.43±0.68
rPOT3	<u>T</u> C ATTGGTGGGTGGGG	rPOT4	<u>T</u> I CATTGGTGGGTGGGG	6.55±0.92
rPOT5	AAT <u>C</u> CTGGTGGGTGGGG	rPOT6	AAT <u>I</u> CTGGTGGGTGGGG	8.91±1.31
rPOT7	<u>T</u> C CATAGGTGGGTGGGG	rPOT8	<u>T</u> G CATAGGTGGGTGGGG	3.10±0.55
rPOT7	<u>T</u> C CATAGGTGGGTGGGG	rPOT9	<u>T</u> C AATAGGTGGGTGGGG	8.32±1.81
rPOT3	<u>T</u> C CATTGGTGGGTGGGG	rPOT10	<u>T</u> A CATTGGTGGGTGGGG	3.10±0.39
rPOT3	<u>T</u> C CATTGGTGGGTGGGG	rPOT11	<u>T</u> C GATTGGTGGGTGGGG	3.39±1.11
rPOT1	AT <u>C</u> CGTGGTGGGTGGGG	rPOT12	AT <u>C</u> AGTGGTGGGTGGGG	2.82±1.34
rPOT13	AT <u>C</u> CGAGGTGGGTGGGG	rPOT14	AT <u>C</u> GAGGTGGGTGGGG	1.63±0.20

ID (Bright)	Sequence (5' → 3')	ID (Dark)	Sequence (5' → 3')	POT difference ratio in yellow channel (Bright/Dark)
rPOT1	AT <u>C</u> CGTGGTGGGTGGGG	rPOT2	AT <u>I</u> CGTGGTGGGTGGGG	0.73±0.07
rPOT3	<u>T</u> C ATTGGTGGGTGGGG	rPOT4	<u>T</u> I CATTGGTGGGTGGGG	1.46±0.24
rPOT5	AAT <u>C</u> CTGGTGGGTGGGG	rPOT6	AAT <u>I</u> CTGGTGGGTGGGG	2.78±0.24
rPOT7	<u>T</u> C CATAGGTGGGTGGGG	rPOT8	<u>T</u> G CATAGGTGGGTGGGG	0.77±0.30
rPOT7	<u>T</u> C CATAGGTGGGTGGGG	rPOT9	<u>T</u> C AATAGGTGGGTGGGG	1.65±0.20
rPOT3	<u>T</u> C CATTGGTGGGTGGGG	rPOT10	<u>T</u> A CATTGGTGGGTGGGG	1.19±0.11
rPOT3	<u>T</u> C CATTGGTGGGTGGGG	rPOT11	<u>T</u> C GATTGGTGGGTGGGG	1.52±0.40
rPOT1	AT <u>C</u> CGTGGTGGGTGGGG	rPOT12	AT <u>C</u> AGTGGTGGGTGGGG	1.59±0.57
rPOT13	AT <u>C</u> CGAGGTGGGTGGGG	rPOT14	AT <u>C</u> GAGGTGGGTGGGG	0.51±0.05

Table S11: Test-tube investigation of yellow POT candidates.

Based on chip selection results, 9 sets of yellow POT candidates are evaluated in test tubes. All these candidates have their POT difference ratios greater than 3.29, with the largest difference ratio of 31.25 (yPOT5/yPOT6 NCBs, Fig. S19). Single-nucleotide differences in these POTs are marked in red.

ID (Bright)	Sequence (5' → 3')	ID (Dark)	Sequence (5' → 3')	POT difference ratio in yellow channel (Bright/Dark)
yPOT1	TAA <u>G</u> TGGGTGGGGTGGGG	yPOT2	TAA <u>C</u> TGGGTGGGGTGGGG	9.16±1.65
yPOT3	TTAGT <u>G</u> GGTGGGGTGGGG	yPOT4	TTAGT <u>C</u> GGTGGGGTGGGG	9.41±0.69
yPOT5	CAGT <u>G</u> AGGTGGGGTGGGG	yPOT6	CAGT <u>C</u> AGGTGGGGTGGGG	31.25±5.37
yPOT7	AGCT <u>G</u> AGGTGGGGTGGGG	yPOT8	AGCT <u>A</u> AGGTGGGGTGGGG	14.17±2.95
yPOT9	ACAG <u>I</u> GGGTGGGGTGGGG	yPOT10	ACAG <u>C</u> GGGTGGGGTGGGG	6.15±1.20
yPOT11	ACAG <u>I</u> GGGTGGGGTGGGG	yPOT12	ACAG <u>A</u> GGGTGGGGTGGGG	3.29±0.26

ID (Bright)	Sequence (5' → 3')	ID (Dark)	Sequence (5' → 3')	POT difference ratio in red channel (Bright/Dark)
yPOT1	TAA <u>G</u> TGGGTGGGGTGGGG	yPOT2	TAA <u>C</u> TGGGTGGGGTGGGG	0.88±0.07
yPOT3	TTAGT <u>G</u> GGTGGGGTGGGG	yPOT4	TTAGT <u>C</u> GGTGGGGTGGGG	0.69±0.24
yPOT5	CAGT <u>G</u> AGGTGGGGTGGGG	yPOT6	CAGT <u>C</u> AGGTGGGGTGGGG	2.10±0.34
yPOT7	AGCT <u>G</u> AGGTGGGGTGGGG	yPOT8	AGCT <u>A</u> AGGTGGGGTGGGG	0.83±0.15
yPOT9	ACAG <u>I</u> GGGTGGGGTGGGG	yPOT10	ACAG <u>C</u> GGGTGGGGTGGGG	0.84±0.07
yPOT11	ACAG <u>I</u> GGGTGGGGTGGGG	yPOT12	ACAG <u>A</u> GGGTGGGGTGGGG	0.68±0.05

Table S12: Machine learning model prediction results

In this report, we evaluated the predictability across various machine learning models, including logistic regression¹⁷ (LR), linear discriminant analysis¹⁸ (LDA), decision tree¹⁹ (DT), AdaBoost²⁰ (ADA), and support vector machines²¹ (SVM). We observed that after feature selection using Weka, LR revealed the best predictability for both the red channel (accuracy: 0.87; marked in red) and yellow channel (accuracy: 0.89; marked in yellow) based on 5-fold cross validation.

Model (red)	Accuracy (Acc)	Sensitivity	Specificity	Positive prediction rate	Negative prediction rate
LR	0.87	0.88	0.85	0.90	0.83
LDA	0.86	0.86	0.85	0.90	0.81
DT	0.84	0.86	0.80	0.86	0.80
ADA	0.86	0.87	0.85	0.90	0.83
SVM	0.86	0.86	0.85	0.90	0.81

Model (yellow)	Accuracy (Acc)	Sensitivity	Specificity	Positive prediction rate	Negative prediction rate
LR	0.89	0.88	0.90	0.92	0.85
LDA	0.87	0.85	0.90	0.92	0.82
DT	0.83	0.84	0.82	0.86	0.79
ADA	0.87	0.86	0.88	0.90	0.83
SVM	0.88	0.87	0.90	0.92	0.84

Table S13: selected bright and dark features for yellow channel

We defined the top 30% as the bright class and bottom 30% as the dark class. The feature extraction was processed using MERCI. We then used Weka to selected important features. The attribute evaluator was set to “CfsSubsetEval”²² and the search method was set to “GreedyStepwise”¹⁵. All other parameters were set to default values.

a Selected bright features (the number indicates the segment that the motif belongs to)

3-nt	4-nt	5-nt	6-nt
	AAGG_1	AG_AG_1	AAG_GT_1
	AGGG_1	CG_AG_1	AAG_GT_3
	AGGG_3	GAGGT_1	CGGG_T_1
	ATGG_1	G_AAG_1	GAGG_G_2
	CGGG_1	G_ATG_1	GA_GGG_2
	GAGG_1	GC_AG_1	GA_GGG_3
	GC GG_1	GCC_G_3	GA_TGG_1
	GTGT_1	GCT_G_3	G_AGTG_1
	TAGG_1	G_CTG_1	GCG_GG_2
	TTGG_1	GGGGG_2	GC_TGG_1
		GT_AG_1	G_CGGT_1
		GTT_G_1	GGA_GG_1
		G_TAG_1	G GC_GG_1
		G_TGT_1	G GCG_GG_2
		TGA_G_1	GGGA_A_1
		TGA_G_2	GGGA_G_1
		TG_AG_1	GGGG_A_1
		T_GCG_3	GGGG_A_3
		TT_GG_1	GG_GCG_1
			G_GGCA_1
			GTGGTG_2
			GTGTGG_3
			GT_TG_1
			GT_TG_3
			GT_TGG_1
			GT_TGG_2
			TGGGTG_1
			TGGGTG_2
			TG_GCG_1
			TTG_GG_2
			TTG_GG_3
			TT_GGT_3

b Selected dark features (the number indicates the segment that the motif belongs to)

3-nt	4-nt	5-nt	6-nt	
AAT_2	ACGT_3	AA(CG_2	AA(TGG_1	GG_GTC_1
ACT_2	CCGG_1	AA_TG_1	AA_TGG_3	GGTGGGA_1
ATC_1	GGAT_1	A_AGT_1	A_AGTG_1	GGTGGGA_2
ATC_2	GGTT_1	AC_CG_2	A_AGTG_2	G_GGAA_1
ATT_2	TCGG_1	AC_TG_1	ACG_GG_1	G_GGAC_1
CAT_2		AT_CG_2	AC_GGT_1	G_GGAT_1
CGC_2		AT_CG_3	AC_GTG_3	G_GGCT_1
CTC_2		ATG_T_1	AC_TGG_1	G_GGTA_1
CTT_3		AT_TG_1	A_CGGT_1	G_GGTC_1
TCA_3		C_AGT_1	ATG_TG_1	G_GGTT_1
TCT_2		C_AGT_2	AT_GGT_1	T_AGTG_2
TTC_2		CCG_T_1	AT_GTG_1	TCGG_G_1
TTT_3		CC_TG_3	CAG_TG_1	TCG_GG_1
		CTC_G_2	CA_GGT_1	TC_TGG_1
		CT_TG_1	CA_TGG_1	T_CGGT_1
		C_TGT_1	C_AGGT_1	TGGA_A_1
		C_TGT_2	C_AGTG_2	TGGA_C_3
		GAT_G_1	CCG_TG_1	TGGA_G_1
		GT_CT_1	CC_GGT_1	TGG_AA_1
		GT_CT_3	CC_TGG_1	TGG_CT_1
		GT_TC_1	CGTGGG_1	TGGT_A_1
		G_TCG_1	CGTGGG_2	TGGT_A_3
		TA_TG_1	CT_GGT_1	TGGT_C_1
		TA_TG_3	CT_TGG_1	TGGT_T_3
		T_AGT_1	C_TGGT_1	TGG_TT_2
		TC_GT_3	C_TGTG_1	TG_GAA_1
		TC_TG_1	C_TGTG_2	TG_GAC_1
		TG_AT_3	G_CGTG_1	TG_GAT_1
		TG_LT_1	G_CGTG_2	TG_GCC_1
		TG_TT_3	GGG_CC_1	TG_GTA_1
		T_GTT_1	GGGT_A_1	TG_GTC_1
		TT_CG_3	GGGT_C_1	TG_GTT_1
		T_TGT_1	GGGT_T_1	T_GGAC_1
				T_GGCC_1
				T_GGCT_1
				T_GGTA_1
				TTG_TG_1

Table S14: selected bright and dark features for red channel

We defined the top 30% as the bright class and bottom 30% as the dark class. The feature extraction was processed using MERCI. We then used Weka to selected important features. The attribute evaluator was set to “CfsSubsetEval” and the search method was set to “GreedyStepwise”. All other parameters were set to default values.

a Selected bright features (the number indicates the segment that the motif belongs to)

3-nt	4-nt	5-nt	6-nt			
CCC_1	AAGG_1	AA_GG_1	AA_GGT_2	CCT_G_3	TA_GGT_2	
CCC_3	ATGG_1	AA_GG_3	ACG_GT_1	C_CAG_3	TC_GGT_1	
	CTGG_3	A_AGG_3	ACG_GT_3	C_CGG_1	TC_GGT_3	
	GAGG_1	ACA_G_1	AC_GGT_2	C_CGG_2	TGGGGG_1	
	GCGG_1	AC_AG_3	AC_GGT_3	C_CTG_1	TGGGGG_3	
	TAGG_1	ACC_G_1	AG_GGT_1	C_CTG_3	TGGGTG_1	
	TTGG_1	AC_GG_2	AG_GGT_2	C_GGG_1	TGGGTG_3	
		ACT_G_1	ATG_GT_3	CT_AG_1	TTGG_G_2	
		ACT_G_3	A_TGGT_2	CT_AG_3	TTG_GT_3	
		A_CCG_1	A_TGGT_3	CTC_G_1	T_TGGT_2	
		A_CCG_3	CAG_GT_3	CTC_G_3	T_TGGT_3	
		A_CGG_1	CCG_GT_3	CT(CG)_1		
		A_CGG_3	CC_GGT_2	CT(CG)_3		
		AT_GG_1	CG_GGT_2	CT_GG_2		
		CAC_G_1	CT_GGT_2	GCC_G_1		
		CAC_G_3	GA_GGT_2	GCC_G_3		
		CA_CG_1	GA_GGT_3	GC_GG_3		
		CA(CG)_3	G_AGGT_1	GGGAC_3		
		CA_GG_1	GC_GGT_2	GGGAA_1		
		CA_GG_2	GC_GGT_3	GGGAA_2		
		C_AGG_2	GGGG_C_3	GGGGAA_3		
		CCA_G_1	GGG_GC_1	GGGGG_1		
		CC_AG_3	GGG_GC_2	TA_GG_3		
		CC_CG_3	GTGGTG_1	T_AGG_3		
		CC_GG_1	GTGGTG_3	TCC_G_1		
		CCT_G_1	TAG_GT_3	TC_CG_1		
				TC_CG_3		
				TC_GG_3		
				T_CCG_3		
				TT_GG_1		
				TT_GG_3		

b Selected dark features (the number indicates the segment that the motif belongs to)

3-nt	4-nt	5-nt	6-nt			
AAA_1	CCGT_1	AA_TG_1	AAGT_G_1	TC_TG_2	GTG_TA_1	
AGA_1	CGTG_3	AGT_G_1	AA_GTG_2	TG_AA_3	GT_GTA_1	
AGA_3	GAGT_1	AGT_G_3	ACG_GG_2	TG_CA_1	GT_GTT_1	
ATA_1	GGAA_1	A_TGT_1	AC_TGG_1	TG(CG)_1	TAC_GG_2	
TAA_1	GGAG_1	CGT_G_1	AC_TGG_2	TG_CT_1	TGG_AA_2	
TGA_1	GGAT_1	CGT_G_2	A_TGGG_2	TGTGG_2	TGG_AC_2	
	GGCA_1	C_TGT_1	CAG_GG_1	TG_TA_3	TGG_AC_3	
	GGCC_1	GAA_C_1	CAG_GG_2	T_GAA_1	TGG_AG_2	
	GGCT_1	GAA_G_3	CAGT_G_1	T_GAC_3	TGG_AT_2	
	GGTA_1	GA_CT_1	CA_TGG_2	T_GAG_3	TGGGTT_1	
	GGTT_1	G_AGC_1	CG_GGG_1	T_GAT_3	TGGGTT_3	
		GCA_G_3	CG_GGG_2	T_GCT_1	TGGT_A_1	
		GCT_G_3	GCG_TG_1	T_GTA_1	TGG_TC_3	
		GC_TC_1	GCG_TG_2	T_GTC_1	TG_GAC_1	
		G_GCC_1	GC_TGG_1	T_GTC_3	TG_GAG_1	
		G_GTC_1	GC_TGG_2	TT_AG_1	TG_GCC_1	
		GTA_G_1	GGGA_A_1	TTC_G_3	TG_GCG_3	
		GT_AT_1	GGG(CG)_1	TT_TG_1	T_GGAA_3	
		GT_CA_1	GGGT_A_1		T_GGTA_3	
		GT_CC_1	GG_GTA_2		T_TGGG_2	
		GT_CT_1	GG_GTT_2		T_TGGG_3	
		GTG_C_2	GGTGGT_1			
		GTGGC_1	GGTGGT_2			
		GT_GA_2	GGTG_T_1			
		G_TTA_1	GGT_TC_1			
		G_TTG_1	GTG_AT_1			
		TAGTG_1	GTGG_C_2			
		TC_TG_1	GTGGGC_3			

References

- 1 Yeh, H. C., Sharma, J., Han, J. J., Martinez, J. S. & Werner, J. H. A DNA-silver nanocluster probe that fluoresces upon hybridization. *Nano Letters* **10**, 3106-3110, doi:10.1021/nl101773c (2010).
- 2 Obliosca, J. M. et al. A complementary palette of NanoCluster Beacons. *ACS Nano* **8**, 10150-10160, doi:10.1021/nn505338e (2014).
- 3 Yeh, H. C. et al. A fluorescence light-up Ag nanocluster probe that discriminates single-nucleotide variants by emission color. *Journal of the American Chemical Society* **134**, 11550-11558, doi:10.1021/ja3024737 (2012).
- 4 Chen, Y. A. et al. NanoCluster Beacons Enable Detection of a Single N(6)-Methyladenine. *Journal of the American Chemical Society* **137**, 10476-10479, doi:10.1021/jacs.5b06038 (2015).
- 5 Zhang, J. et al. Hairpin DNA-Templated Silver Nanoclusters as Novel Beacons in Strand Displacement Amplification for MicroRNA Detection. *Analytical Chemistry* **88**, 1294-1302, doi:10.1021/acs.analchem.5b03729 (2016).
- 6 Jung, C. et al. Massively Parallel Biophysical Analysis of CRISPR-Cas Complexes on Next Generation Sequencing Chips. *Cell* **170**, 35-47, doi:10.1016/j.cell.2017.05.044 (2017).
- 7 McGinnis, A. C., Grubb, E. C. & Bartlett, M. G. Systematic optimization of ion-pairing agents and hexafluoroisopropanol for enhanced electrospray ionization mass spectrometry of oligonucleotides. *Rapid Commun Mass Spectrom* **27**, 2655-2664, doi:10.1002/rcm.6733 (2013).
- 8 Sutton, J. M. & Bartlett, M. G. Modeling cationic adduction of oligonucleotides using electrospray desorption ionization. *Rapid Commun Mass Spectrom* **34**, e8696, doi:10.1002/rcm.8696 (2020).
- 9 Sutton, J. M., El Zahar, N. M. & Bartlett, M. G. Oligonucleotide Anion Adduct Formation Using Negative Ion Electrospray Ion-Mobility Mass Spectrometry. *J Am Soc Mass Spectrom* **32**, 497-508, doi:10.1021/jasms.0c00380 (2021).
- 10 Scalabrin, M., Palumbo, M. & Richter, S. N. Highly Improved Electrospray Ionization-Mass Spectrometry Detection of G-Quadruplex-Folded Oligonucleotides and Their Complexes with Small Molecules. *Anal Chem* **89**, 8632-8637, doi:10.1021/acs.analchem.7b01282 (2017).
- 11 Copp, S. M., Bogdanov, P., Debord, M., Singh, A. & Gwinn, E. Base motif recognition and design of DNA templates for fluorescent silver clusters by machine learning. *Advanced Materials* **26**, 5839-5845, doi:10.1002/adma.201401402 (2014).
- 12 Copp, S. M. et al. Fluorescence Color by Data-Driven Design of Genomic Silver Clusters. *ACS Nano*, doi:10.1021/acsnano.8b03404 (2018).
- 13 Copp, S. M., Swasey, S. M., Gorovits, A., Bogdanov, P. & Gwinn, E. G. General Approach for Machine Learning-Aided Design of DNA-Stabilized Silver Clusters. *Chemistry of Materials* **32**, 430-437, doi:10.1021/acs.chemmater.9b04040 (2019).
- 14 Vens, C., Rosso, M. N. & Danchin, E. G. Identifying discriminative classification-based motifs in biological sequences. *Bioinformatics* **27**, 1231-1238, doi:10.1093/bioinformatics/btr110 (2011).

- 15 Hall, M. *et al.* The WEKA data mining software. *ACM SIGKDD Explorations Newsletter* **11**, 10-18, doi:10.1145/1656274.1656278 (2009).
- 16 Ristad, E. S. & Yianilos, P. N. Learning string-edit distance. *IEEE Transactions on Pattern Analysis and Machine Intelligence* **20**, 522-532, doi:10.1109/34.682181 (1998).
- 17 Menard, S. Applied Logistic Regression Analysis. doi:10.4135/9781412983433 (2002).
- 18 Mika, S., Ratsch, G., Weston, J., Scholkopf, B. & Mullers, K. R. Fisher discriminant analysis with kernels. *Neural Networks for Signal Processing IX: Proceedings of the 1999 IEEE Signal Processing Society Workshop (Cat. No.98TH8468)*, 41-48, doi:10.1109/NNSP.1999.788121 (1999).
- 19 Safavian, S. R. & Landgrebe, D. A survey of decision tree classifier methodology. *IEEE Transactions on Systems, Man, and Cybernetics* **21**, 660-674, doi:10.1109/21.97458 (1991).
- 20 Freund, Y. & Schapire, R. E. A Decision-Theoretic Generalization of On-Line Learning and an Application to Boosting. *Journal of Computer and System Sciences* **55**, 119-139, doi:10.1006/jcss.1997.1504 (1997).
- 21 Cortes, C. & Vapnik, V. Support-vector networks. *Machine Learning* **20**, 273-297 (1995).
- 22 Hall, M. A.; Smith, L. A. Practical Feature Subset Selection for Machine Learning. In Proceedings of the 21st Australasian Computer Science Conference ACSC'98; Springer, Berlin, Heidelberg: Perth, 1998; pp 181–191.